The Dissertation Committee for Dario Fernando Martinez Mantilla certifies that this is the approved version of the following dissertation:

Floquet theory and continued fractions for harmonically driven systems

Committee:

Linda Reichl, Supervisor

Alejandro De Lozanne

Tommio Petrosky

Robert Wyatt

Peter Antoniewicz

Floquet theory and continued fractions for harmonically driven systems

by

Dario Fernando Martinez Mantilla, B.S.

DISSERTATION

Presented to the Faculty of the Graduate School of

The University of Texas at Austin

in Partial Fulfillment

of the Requirements

for the Degree of

DOCTOR OF PHILOSOPHY

THE UNIVERSITY OF TEXAS AT AUSTIN

August 2003

Para Noemi.

Acknowledgments

I would like to thank all of the people who have helped me in so many ways during this awesome 7 years in Austin. I specially wish to name those without whom I would not be graduating: Thanks to Dr. L.E. Reichl for her advise and support. To German Luna-Acosta for many invitations to come see him in Puebla, for the many enjoyable discussions about physics and everything else, and above all, for his friendship. To Annie Harding and Norma Kotz, for their patience, their efficiency and constant willingness to help. To Anne and Roger Chenu, my adoptive parents, for accepting me as one of their own, for all their help and emotional and material support. To my family for their unconditional love. To all my friends for their friendship and support. And finally, thank you Noemi, my wonderful partner in this journey and the ones to come.

Floquet theory and continued fractions for harmonically driven systems

Publication No. _____

Dario Fernando Martinez Mantilla, Ph.D.
The University of Texas at Austin, 2003

Supervisor: Linda Reichl

We derive an exact solution using continued fractions for a quantum particle scattering from an oscillating delta-function potential. We study its transmission properties such as: Transmission zeros, transmission poles and threshold anomalies. Using the same technique and a translation matrix method, we study the problem of an infinite chain of oscillating deltas. We calculate its band structure and eigenstates and show explicitly the contribution to these eigenstates from the quasi-bound state of a single oscillating delta. We study the dynamics of the quasi-energy bands of the system as a function of the strength of the oscillation and show band quasi-periodicity and band collapse. We also define the Floquet-Green's function for a time-periodic Hamiltonian and by a generalization of the method used for the two previous potentials we are able to derive an expression for the Floquet-Green's function of any harmonically driven Hamiltonian. As an example of the application of this method we study a tight-binding Hamiltonian with harmonic time dependence.

Table of Contents

List of Tables

List of Figures

Chapter 1

Introduction

The study of the effect of periodic driving in a system is among the oldest in physics. The study of resonance, as it occurs in so many different physical systems, from musical instruments to planetary motion, plays a central role in the development of classical mechanics. With the discovery of electromagnetic induction and Maxwell's equations, a description of the interaction between matter and electromagnetic radiation became possible; once again, central to this description lies the understanding of the effects of a harmonic drive in the atomic states. Furthermore, in the field of solid state, a microscopic description of electrons inside a crystal requires the study of the effect on the electron's motion due to the interaction between them and the vibrations in the atomic potentials due to thermal fluctuations. These vibrations, which have a well defined frequency, can be thought to act, within the classical approximation, as harmonically driven potentials in the electron's Hamiltonian. Therefore, the study of harmonically driven Hamiltonians is of significant importance because of the enormous field of applications in solid state, atomic physics, and many other fields.

The theory of homogeneous linear differential equations with periodic

coefficients dates back to 1877 when G.W. Hill[1] published a remarkable memoir on the motion of the moon's perigee. In that paper, Hill studied the equation that now bears his name:

$$-\frac{\partial^2\phi}{\partial t^2} + V(t)\phi = \lambda\phi, \qquad V(t) = V(t+\tau) \tag{1.1}$$

The periodicity of the potential $V(t)$ in Hill's original paper is due to the periodic motion of the reduced earth-sun system. This same equation occurs in many places in the physical sciences: In models of parametric resonance, as a description of electrons in a crystalline lattice, in Riemannian geometry describing the Jacobi fields of variations of periodic geodesics, even in the reheating problem of the inflationary universe [5], among others. Equation 1.1 is notable for its spectrum of stable bands alternating with 'gaps' or regions of instability.

Hill assumed that this differential equation had solutions of the form $x = e^{\varepsilon t}y(t)$ with $y(z(t))$ and $z(t) = e^{it}$. He then expressed $y(z)$ and the periodic coefficients, $V(t)$ in the equation, in a Laurent series in z. By equating the (infinite) determinant of the coefficients to zero, an equation is obtained for the values of ε that satisfy the differential equation. Hill introduced for the first time in mathematics the infinite determinant, which was later studied by Poincaré and others.

In 1883, G. Floquet published [3] a complete discussion of the properties of the solutions of a linear differential equation of the n^{th} order with periodic coefficients. The general properties of the solutions having been determined,

later authors devoted considerable attention to the problem of discovering practical methods of obtaining them.

In Quantum Mechanics, Hill's equation appears for the first time in 1928 with Bloch's theory of electrons in a crystal [4]. The spatial periodicity in this case is due to the atomic potentials. It is interesting to mention that in his paper, there was no mention to any of the mathematical work on differential equations with periodic coefficients that had been developed in the previous 50 years. Bloch derives his theorem for a periodic three dimensional space and also studied the effect of an electric field in an electron moving through the crystal. After this paper, Bloch's theorem became a corner-stone in solid state physics and his name is forever associated with space periodic potentials in quantum physics.

Possibly, because of Bloch's omission, Floquet's name only appears significantly in the physics of the last 35 years. This is when efforts began to obtain more accurate descriptions of systems interacting with a classical field that is periodic in time. An example of this is an AC electric field and systems interacting with electromagnetic radiation.

Even though an exact treatment of such systems has to be formulated using Floquet's Theory, up to the 1960's such systems where studied using only perturbative approaches, most famously the Rotating Wave Approximation (RWA) which allows one to get results analytically. In such an approach, the strength of the oscillating field is assumed to be small and the frequency of the oscillation is assumed to be resonant with the transition frequency of the

system (typically a two state system).

With technological advances making possible the use of very strong electromagnetic fields, non-perturbative approaches have become very important and Floquet's theory is now widely used. Of particular importance for its development are the papers by Shirley [52] and Sambe[6]. The first one uses Floquet's theory to solve the important problem of a two state system interacting with a periodic field. In Sambe's paper a general formalism is developed in which he introduces an extended Hilbert space that allows one to formally treat the original time-dependent system as a time independent one, for which the tools developed for time-independent systems can be used.

Along this same line of thought, a more recent development is the t-t' method [7] which goes a step further in this direction, by developing a formalism which treats, on equal footing, the scattering through a time independent and a time-dependent potential. Its basic idea is to introduce an auxiliary variable t' which extends the Hilbert space of the system so that the real time dependence of the Hamiltonian can be addressed using the traditional methods of time-independent scattering. It basically provides a method to go from a time dependent system with n dimensions to a time-independent system with n+1 dimensions. We can therefore say that this method formally brings to Quantum Mechanics a trick that has been used in classical mechanics for many years. One of the interesting things about this method is that it applies to any time-dependent potential, including as a special case periodic time dependence. With this new approach the problem of time-ordering in the

calculation of an evolution operator becomes obsolete.

Our contributions in this dissertation consist of the application of Floquet's theory to the exact solution of two particular time-periodic problems (Chapters 2 & 3) and the introduction of the Floquet-Green's function for a general time-periodic potential as well as the development of a simple method for its calculation in the case of a general potential with a harmonic dependence on time (Chapter 4).

In what remains of this chapter we will introduce the reader to the two main mathematical tools that are used throughout this work.

1.1 Floquet's theorem

Floquet's theorem, in the context of Quantum Mechanics and just like Bloch's theorem, claims that a periodicity in the Hamiltonian produces a quasi-periodicity in the solutions to Schrödinger's equation (the time independent one for Bloch's, the time dependent one for Floquet's) . In this respect one might be tempted to say that they are the same theorem. That is really not the case since there are many differences worth mentioning: In Bloch's theorem, the Hamiltonian is periodic in the space coordinates and required to be time independent; in Floquet's theorem the Hamiltonian is time periodic, and we require nothing about its space dependence. Bloch's theorem is derived on a differential equation that is second order in a coordinate in space (kinetic energy term), which is also the variable that is periodic; in Floquet's case the differential equation is first order in the variable that is periodic (time).

Bloch's equation is an eigenvalue equation, Floquet's is not (a corollary of Floquet's theorem is that you can arrive to an eigenvalue equation, but that is a consequence, not a starting point in proving it). Because of these differences, we have included here, for completeness, a proof of Floquet's theorem. It is also included here because the proof is never included in Quantum Mechanics books and the reader is not likely to have seen it before.

In what follows we will use the notation that capitalized letters correspond to operators, and non-capitalized correspond to functions of position and time (x,t). We have chosen the x-representation for all the operators.

Explicitly, Floquet's theorem states that if

$$\mathcal{H}(x,t) = \mathcal{H}(x,t+\tau) \tag{1.2}$$

then, the solutions to Schrödinger's equation are of the form

$$\psi_\varepsilon(x,t) = e^{-i\varepsilon t}\phi_\varepsilon(x,t) \tag{1.3}$$

where $\phi_\varepsilon(x,t) = \phi_\varepsilon(x,t+\tau)$.

We start with Schrödinger's equation

$$i\hbar\frac{\partial\psi}{\partial t}(x,t) = \mathcal{H}(x,t)\psi(x,t), \tag{1.4}$$

and define the time-translation operator $\mathcal{U}(x,t)$ as $\psi(x,t) = \mathcal{U}(x,t)\psi(x,0)$. $\mathcal{U}(x,t)$ satisfies

$$i\hbar\frac{\partial}{\partial t}\mathcal{U}(x,t) = \mathcal{H}(x,t)\mathcal{U}(x,t). \tag{1.5}$$

We now define the operator

$$\Lambda_\tau(x) \equiv \mathcal{U}^{-1}(x,t)\mathcal{U}(x,t+\tau), \tag{1.6}$$

from which

$$\mathcal{U}(x,t+\tau) = \mathcal{U}(x,t)\Lambda_\tau(x). \tag{1.7}$$

Since Λ_τ is not singular (i.e. it has an inverse), we can always find an operator $\mathcal{W}(x)$ that satisfies $\Lambda_\tau(x) = e^{-\frac{i}{\hbar}\tau\mathcal{W}(x)}$. Notice that $\mathcal{W}$ must be Hermitian since Λ_τ is unitary. We now write the time propagator as

$$\mathcal{U}(x,t) = \Phi(x,t)e^{-\frac{i}{\hbar}t\mathcal{W}(x)}. \tag{1.8}$$

and prove that $\Phi(x,t+\tau) = \Phi(x,t)$. From the previous equation evaluated at $t+\tau$ we get

$$\mathcal{U}(x,t+\tau) = \Phi(x,t+\tau)e^{-\frac{i}{\hbar}t\mathcal{W}(x)}e^{-\frac{i}{\hbar}\tau\mathcal{W}(x)}; \tag{1.9}$$

also, from the definition of Λ_τ

$$\mathcal{U}(x,t+\tau) = \mathcal{U}(x,t)\Lambda_\tau(x) = \Phi(x,t)e^{-\frac{i}{\hbar}t\mathcal{W}(x)}e^{-\frac{i}{\hbar}\tau\mathcal{W}(x)}. \tag{1.10}$$

From this we conclude that $\Phi(x,t+\tau) = \Phi(x,t)$.

The solutions to Schrödinger's equation can therefore be written as

$$\psi(x,t) = \mathcal{U}(x,t)\psi(x,0) = \Phi(x,t)e^{-\frac{i}{\hbar}t\mathcal{W}(x)}\psi(x,0). \tag{1.11}$$

If $\psi(x,0) = \nu_\varepsilon(x)$, with $\nu_\varepsilon(x)$ being an eigenfunction of $\mathcal{W}(x)$ with eigenvalue ε, the corresponding wave-function is

$$\psi_\varepsilon(x,t) = e^{-\frac{i}{\hbar}t\varepsilon}\Phi(x,t)\nu_\varepsilon(x) \tag{1.12}$$

or

$$\psi_\varepsilon(x,t) = e^{-\frac{i}{\hbar}t\epsilon}\phi_\varepsilon(x,t), \tag{1.13}$$

with $\phi_\epsilon(x,t)$ a periodic function of time. The periodic functions $\phi_\varepsilon(x,t)$ can be calculated from an eigenvalue equation if we substitute Eq.1.13 into Schrödinger's equation

$$\begin{aligned} i\hbar\frac{\partial}{\partial t}\psi_\varepsilon(x,t) &= i\hbar\frac{\partial}{\partial t}e^{-\frac{i}{\hbar}t\epsilon}\phi_\varepsilon(x,t) \\ &= \varepsilon e^{-\frac{i}{\hbar}t\epsilon}\phi_\varepsilon(x,t) + i\hbar e^{-\frac{i}{\hbar}t\epsilon}\frac{\partial}{\partial t}\phi_\varepsilon(x,t) \\ &= \mathcal{H}(x,t)e^{-\frac{i}{\hbar}t\epsilon}\phi_\varepsilon(x,t). \end{aligned} \tag{1.14}$$

Cancelling $e^{-\frac{i}{\hbar}t\epsilon}$ everywhere, we can write the last equality as an eigenvalue equation

$$\mathcal{H}^F(x,t)\phi_\varepsilon(x,t) = \varepsilon\phi_\varepsilon(x,t), \tag{1.15}$$

where the Floquet Hamiltonian $\mathcal{H}^F$ is defined as

$$\mathcal{H}^F(x,t) \equiv \mathcal{H}(x,t) - i\hbar\frac{\partial}{\partial t}. \tag{1.16}$$

In Schrödinger's equation the time variable is just a parameter that labels the different wave-functions that describe the state of the system at different times. These wave-functions belong to the Hilbert space ($\mathcal{R}$) of the system which is defined as the set of all square integrable functions $f(\vec{r})$ with finite $\int |f(\vec{r})|^2 d\vec{r}$ and inner product $< f, g > \equiv \int f^*(\vec{r})g(\vec{r})d\vec{r}$. Where $\vec{r}$ is in

the configuration space of the system. This Hilbert space has an orthonormal basis denoted by $\{f_1(\vec{r}), f_2(\vec{r}), ...\}$

Because Eq. 1.15 is an eigenvalue equation, time appears not as the evolution parameter but as a variable that describes the state of the system (!) Clearly the Hilbert space in which the solutions of such equation live must be extended to include the parameter 'time' along with the coordinates in configuration space. For this purpose we follow Sambe's [6] original paper: Let us call $\mathcal{T}$ the Hilbert space of all possible periodic functions $a(t)$ of time, with period τ and finite $\int_{-\tau/2}^{\tau/2} |a(t)|^2 dt$, which is also furnished with the inner product $(a,b) \equiv \frac{1}{\tau}\int_{-\tau/2}^{\tau/2} a^*(t)b(t)dt$. The functions $e^{iq\omega t}$, for q any integer, and $\omega = 2\pi/\tau$ form a complete orthonormal set in the Hilbert space $\mathcal{T}$.

We construct now the composite Hilbert space $\mathcal{R}+\mathcal{T}$ consisting of all possible functions $u(\vec{r},t)$ which are periodic in time with period τ and for which $\int_{-\tau/2}^{\tau/2}\int |u(\vec{r},t)|^2 d\vec{r}dt$ is finite. $\vec{r}$ is in the configuration space of the system as before. The inner product between functions $u(\vec{r},t)$ and $v(\vec{r},t)$ in this space is defined as $<< u,v >> \equiv \frac{1}{\tau}\int_{-\tau/2}^{\tau/2}\int u^*(\vec{r},t)v(\vec{r},t)d\vec{r}dt$. The functions $u_{n,q}(\vec{r},t) \equiv f_n(\vec{r})e^{iq\omega t}$, $n = 1,2,.....$, $q = 0,\pm 1,\pm 2,....$ form a complete orthonormal set of this Hilbert space.

A Hermitian operator $\mathcal{A}$ in $\mathcal{R}+\mathcal{T}$ is defined as an operator which satisfies $<< u,\mathcal{A}v >> = << \mathcal{A}u, v >>$ for any function $u(\vec{r},t)$ and $v(\vec{r},t)$ in $\mathcal{R}+\mathcal{T}$. Any Hermitian operator in $\mathcal{R}$ or $\mathcal{T}$ is also Hermitian in $\mathcal{R}+\mathcal{T}$. Since $\mathcal{H}$ is Hermitian in $\mathcal{R}$ (and therefore in $\mathcal{R}+\mathcal{T}$), and also $i\hbar\frac{\partial}{\partial t}$ is Hermitian in $\mathcal{T}$ (and therefore in $\mathcal{R}+\mathcal{T}$), it follows that $\mathcal{H}^F$ is a Hermitian operator in $\mathcal{R}+\mathcal{T}$.

An interesting thing to point out is that, since the operators $\mathcal{W}$ and $\mathcal{H}^F$ have the same set of eigenvalues and are both Hermitian, one might be tempted to say that they are the same operator. This, however, cannot be possible. $\mathcal{H}^F$ is Hermitian in $\mathcal{R}+\mathcal{T}$, but it is *not* Hermitian in $\mathcal{R}$. Ignoring this basic difference can lead to nonsense. For example, if we assume they are the same operator, then the operator $\Lambda(x) = e^{-\frac{i}{\hbar}\tau\mathcal{W}(x)} = e^{-\frac{i}{\hbar}\tau(\mathcal{H}(x,t)-i\hbar\frac{\partial}{\partial t})}$ acting on a solution to Schrödinger's equation $\psi(x,t)$ becomes the identity since $(\mathcal{H}(x,t) - i\hbar\frac{\partial}{\partial t})\psi(x,t) = 0$.

1.2 Continued Fractions

A continued fraction (CF) is simply a number of the form

$$f = a_0 + \cfrac{b_1}{a_1 + \cfrac{b_2}{a_2 + \cfrac{b_3}{\vdots}}}$$

where the fraction can contain a finite or an infinite number of a's and b's. The truncation of the continued fraction after the step n-th is called the n-th convergent(f_n) of the fraction,

$$f_n = a_0 + \cfrac{b_1}{a_1 + \cfrac{b_2}{a_2 + \cfrac{b_3}{\ddots \cfrac{}{a_{n-1} + \cfrac{b_n}{a_n}}}}}$$

Formally, the infinite continued fraction f is the limit of the sequence of convergents $f_0, f_1, f_2, ...$

The convergence of continued fractions is a very rich topic beyond the scope of this work; suffice it to say that in all cases studied here, convergence was always checked and achieved.

The history of continued fractions[8] is certainly one of the longest among those of mathematical concepts. It begins twenty three centuries ago with Euclid's algorithm for the greatest common divisor. Even though from Euclid's algorithm one can get the ratio of two numbers as a continued (finite) fraction there is no evidence that the Greeks ever used it to form a continued fraction. A little more recently, we have the Rhind mathematical papyrus from Egypt (1600 B.C.), where ascending continued fractions are written. The first attempt to get a general definition of a CF was made by the merchant Leonardo of Pisa, also called Fibonacci(1170-1250). The first known use of a CF as an approximate expression for an irrational number

$$\sqrt{13} \cong 3 + \frac{4}{6 + \frac{4}{6}}$$

was given by the Italian R. Bombelli in 1572. Later, his compatriot Cataldi (1613) would synthesize Bombelli's method. The first infinite CF expansion is due to Lord W. Brouncker (1620-1686) who was the first president of the Royal Society of London. Around 1659 he obtained

$$\frac{4}{\pi} = 1 + \cfrac{1}{2 + \cfrac{3^2}{2 + \cfrac{5^2}{\ddots}}}.$$

The beginning of the theory of CFs is due mostly to Wallis (1657) and Huygens (1682). The golden age in the study of CFs was the 18th century with

the contribution from some of the greatest mathematicians of that era: Euler(1731), Lambert (1750) and Lagrange (1766) (all from the Berlin Academy of Science). Also in that century, Padé approximants were developed, which are closely connected to CFs and play an important role in applications in many fields.

The nineteenth century was a popular period for CFs. The subject was know to every mathematician and even every scholar in many countries. An army of mathematicians, including the most famous ones, contributed to the development of the theory of continued fractions and their application to various problems in mathematics and physics.

Since then, CFs have played a very important role in the development of many branches of mathematics (e.g. the famous proof of the transcendence of π in 1882 was obtained using CFs) and have been used extensively in computer science, electronics, physics, etc...

One of the main reasons why continued fractions are so useful in computation is that they often provide representations for transcendental functions that are much more generally valid than the classical representation by a power series. As mentioned before they are related to the theory of how to approximate functions with ratios of two polynomials (rational approximation or Padé approximation).

In Physics they have been used mainly for the solution of three-term recursion relations, either in functions or in operators. Such is the case for tight-

binding Hamiltonians [9, 10], for the time-independent Schrödinger equation (in discretized space) [11], and for harmonic time-dependent potentials, such as an atom in a standing-wave laser field [12, 13] or for tunneling in the presence of phonons [14]. Continued fractions have also been used in Classical Mechanics to approximate irrational winding numbers for the study of KAM torus and the conditions for its destruction[15].

CF methods are numerically effective, because of their recursiveness; non-perturbative, in the sense that they do not approximate a function as a finite power series, and analytical, since exact analytic results, although often difficult, are possible.

Floquet's theorem and continued fractions are the two fundamental tools that will be used throughout this work.

Chapter 2

Transmission Properties of the oscillating delta-function potential

2.1 Introduction

Time-dependent potentials in mesoscopic systems have been studied for a number of years in connection with electron-phonon interactions [14], quantum tunneling time [16–18], ionization [19, 20], electronic transmission [21–24] and also in the field of quantum chaos [15]. One of the interesting features of localized time-periodic potentials is the presence of resonances or quasi-bound "states", which could be thought of as electrons dynamically trapped by the oscillating potential. This is also a feature common to all multi-channel quantum scattering problems [25, 26].

We first prove here, starting from Schrödinger's equation, that the transmission amplitude has the structure of a CF of functions of the incident energy and the strength of the delta potential. This is a considerable advantage over the numerical computation of the transmission done before using this kind of potential [21, 22]. Our expression allows us to study with greater detail, both analytically and numerically, several different features of the transmission that had not been noticed or explained before, such as the

location of the zero-pole resonances of the transmission and the almost periodic behavior of their position, the existence of non-resonant "bands", the dependence of the pole residues on energy and the existence of the so-called (in the language of nuclear physics) "threshold anomalies" in the transmission. We believe our work gives some insight and clarifies issues in the general problem of scattering through harmonically driven localized potentials. One such potential is the Landau-Büttiker potential, for which numerical and analytical studies of the transmission have been done [23, 24], showing many similarities with the transmission properties of the potential studied in this paper.

In Section 2.2 we use Floquet's theorem to derive the equations that couple different components of the wave function in a plain wave basis, and then we use these equations to find the S-matrix for this potential. In Section 2.3 we solve the equations derived in Section 2.2 and find the exact CF expression for the transmission amplitudes. In Section 2.4 and 2.5 we study analytically and numerically the zeros and poles of the transmission. In Section 2.6 we briefly discuss the "threshold anomalies" in the transmission amplitude.

2.2 Scattering Matrix and Transmission Amplitudes

A formal treatment of the problem of scattering by a time-periodic potential can be found in [23, 27]. Also, a discussion about the sub-space of the Hilbert space suitable for the treatment of time-periodic potentials can be found in [6].

The Hamiltonian we consider is

$$H(x,t) = -\frac{\hbar^2}{2\mu}\frac{d^2}{dx^2} + V\delta(x)\cos(\omega t), \tag{2.1}$$

where μ is the mass of the particle. Even though energy is not conserved, the quasi-energy, ε, is conserved for this system and takes on a continuous range of values in the interval $0 \leq \varepsilon \leq \hbar\omega$. The Floquet eigenstate with quasi-energy, ε, takes the form

$$\Psi_\varepsilon(x,t) = \sum_{n=-\infty}^{\infty} \psi_n(x) e^{-\frac{i}{\hbar}(\varepsilon + n\hbar\omega)t}. \tag{2.2}$$

Since the potential is zero everywhere except at $x = 0$, we assume $\psi_n(x)$ to be of the form

$$\begin{aligned} {\psi_n}^L(x) &= \frac{1}{\sqrt{k_n}}(a_n e^{ik_n x} + d_n e^{-ik_n x}) \quad \text{for } x < 0 \\ {\psi_n}^R(x) &= \frac{1}{\sqrt{k_n}}(c_n e^{ik_n x} + b_n e^{-ik_n x}) \quad \text{for } x > 0. \end{aligned} \tag{2.3}$$

The factor $\frac{1}{\sqrt{k_n}}$ has been included to ensure unitarity of the S-matrix and the wave-vectors k_n are defined by

$$k_n = \sqrt{\frac{2\mu}{\hbar^2}(\varepsilon + n\hbar\omega)} \tag{2.4}$$

In this paper n will always have the range $-\infty < n < \infty$. The square root function has its branch cut on the real energy axis (so that a real energy gives a real momentum). For the energy on the negative real axis we will use the Riemann sheet that has $Im(k_n) \geq 0$, the so called "physical sheet". On this sheet the momentum k_n is on the positive imaginary axis for any $n < 0$. This is required to allow for evanescent modes (exponentially decaying on both sides

of the potential) since they can contribute significantly to the wave-function in the neighborhood of the delta function. These evanescent states are also related to resonances or quasi-bound states which are known to exist in multi-channel problems. To avoid any unphysical exponentially growing states when dealing with positive pure imaginary momentum states, we will require that $a_n = 0$ and $b_n = 0$ for $n \leq -1$. To study the resonances in the transmission we will allow the energy to take complex values and will not necessarily stay on the physical sheet. This will be discussed in section 2.5.

The Floquet eigenstate, $\Psi_\varepsilon(x,t)$, must be continuous at $x = 0$. This leads to the condition

$$a_n + d_n = c_n + b_n. \tag{2.5}$$

Because of the delta function in the Hamiltonian, the slope of $\Psi_\varepsilon(x,t)$ is discontinuous and satisfies

$$d\Psi_\varepsilon dx\Big|_{x=0^+} - d\Psi_\varepsilon dx\Big|_{x=0^-} = \frac{2\mu V}{\hbar^2}\cos(\omega t)\Psi_\varepsilon(0,t). \tag{2.6}$$

This leads to the condition

$$c_n + d_n - b_n - a_n = -2i\ [h_{n-1}(a_{n-1} + d_{n-1}) + h_n(a_{n+1} + d_{n+1})], \tag{2.7}$$

where

$$h_n = \frac{\mu V}{2\hbar^2\sqrt{k_n k_{n+1}}}. \tag{2.8}$$

We can now combine Eqs. (2.5) and (2.7), to obtain the following relations between coefficients

$$c_n + ih_n c_{n+1} + ih_{n-1}c_{n-1} = a_n - ih_n b_{n+1} - ih_{n-1}b_{n-1} \tag{2.9}$$

and

$$d_n + ih_n d_{n+1} + ih_{n-1} d_{n-1} = b_n - ih_n a_{n+1} - ih_{n-1} a_{n-1}. \tag{2.10}$$

It is useful to separate the propagating modes from the evanescent modes. Let us define column vectors

$$\bar{c}_p = \begin{pmatrix} c_0 \\ c_1 \\ c_2 \\ \vdots \end{pmatrix} \quad \text{and} \quad \bar{c}_e = \begin{pmatrix} c_{-1} \\ c_{-2} \\ c_{-3} \\ \vdots \end{pmatrix}, \tag{2.11}$$

where $\bar{c}_p$ contains the amplitudes of the propagating modes outgoing to the right, and $\bar{c}_e$ contains the amplitudes of the evanescent modes that decay to the right. Analogous definitions apply for the column vectors $\bar{a}_p$, $\bar{b}_p$, $\bar{d}_p$, and $\bar{d}_e$. Note that $\bar{a}_e \equiv \bar{0}$ and $\bar{b}_e \equiv \bar{0}$. We can now rewrite Eqs. (2.9) and (2.10) in the following form

$$\begin{aligned}
(\bar{1}_{pp} + \bar{X}_{pp})\cdot\bar{c}_p + \bar{X}_{pe}\cdot\bar{c}_e &= \bar{a}_p - \bar{X}_{pp}\cdot\bar{b}_p, \\
\bar{X}_{ep}\cdot\bar{c}_p + (\bar{1}_{ee} + \bar{X}_{ee})\cdot\bar{c}_e &= -\bar{X}_{ep}\cdot\bar{b}_p, \\
(\bar{1}_{pp} + \bar{X}_{pp})\cdot\bar{d}_p + \bar{X}_{pe}\cdot\bar{d}_e &= \bar{b}_p - \bar{X}_{pp}\cdot\bar{a}_p, \\
\bar{X}_{ep}\cdot\bar{d}_p + (\bar{1}_{ee} + \bar{X}_{ee})\cdot\bar{d}_e &= -\bar{X}_{ep}\cdot\bar{a}_p,
\end{aligned} \tag{2.12}$$

where $\bar{1}_{pp}$ and $\bar{1}_{ee}$ are infinite dimensional unit matrices and matrices $\bar{X}_{pp}$, $\bar{X}_{ee}$, $\bar{X}_{ep}$, and $\bar{X}_{pe}$ have matrix elements

$$\begin{aligned}
(\bar{X}_{pp})_{m,m'} &= ih_m\ (\delta_{m,m'+1} + \delta_{m,m'-1}), \quad & (\bar{X}_{ee})_{\nu,\nu'} &= ih_\nu\ (\delta_{\nu,\nu'+1} + \delta_{\nu,\nu'-1}), \\
(\bar{X}_{pe})_{m,\nu} &= ih_{-1}\ \delta_{m,0}\delta_{\nu,-1}, & (\bar{X}_{ep})_{\nu,m} &= ih_{-1}\ \delta_{m,0}\delta_{\nu,-1}.
\end{aligned} \tag{2.13}$$

Note that we have introduced the convention that the indices $m = 0, 1, 2, .., \infty$, and $\nu = -1, -2, -3.., -\infty$, to help separate propagating modes from evanescent modes.

We can now write the scattering matrix for this system. The scattering matrix, $\bar{S}$, connects the incoming propagating modes to the outgoing propagating modes

$$\begin{pmatrix} \bar{d}_p \\ \bar{c}_p \end{pmatrix} = \bar{S} \cdot \begin{pmatrix} \bar{a}_p \\ \bar{b}_p \end{pmatrix} = \begin{pmatrix} \bar{r} & \bar{t}' \\ \bar{t} & \bar{r}' \end{pmatrix} \cdot \begin{pmatrix} \bar{a}_p \\ \bar{b}_p \end{pmatrix}, \tag{2.14}$$

where $\bar{t}$ and $\bar{t}'$ are matrices of transmission probability amplitudes and $\bar{r}$ and $\bar{r}'$ are matrices of reflection probability amplitudes. More specifically, the matrix element $t_{m,m'} = (\bar{t})_{m,m'}$ is the probability amplitude for the m' mode entering from the left to transmit to the right, and $r_{m,m'} = (\bar{r})_{m,m'}$ is probability amplitude that the m' mode entering from the left and will reflect to the left. Matrix elements of $\bar{r}'$ and $\bar{t}'$ contain reflection and transmission coefficients for modes entering from the right. After some algebra one can show that

$$\bar{t} = \bar{t}' = (\bar{1}_{pp} + \bar{Y}_{pp})^{-1} \quad \text{and} \quad \bar{r} = \bar{r}' = -(\bar{1}_{pp} + \bar{Y}_{pp})^{-1} \cdot \bar{Y}_{pp}, \tag{2.15}$$

where

$$\bar{Y}_{pp} = \bar{X}_{pp} - \bar{X}_{pe} \cdot (\bar{1}_{ee} + \bar{X}_{ee})^{-1} \cdot \bar{X}_{ep}. \tag{2.16}$$

The effects of the evanescent modes are now explicitly included in the scattering matrix.

For propagating modes entering in the m^{th} channel on the left, the total

probability for transmission to the right is

$$T_m = \sum_{m'=0}^{\infty} |t_{m',m}|^2. \tag{2.17}$$

In the next section we focus on the transmission probability, T_0. By expanding it in continued fractions, we can determine all the transmission zeros and complex poles of this system.

2.3 Continued fractions solution

Let us now consider the special case of a single propagating mode, entering in channel $m = 0$ from the left and no propagating modes entering from the right. In this case $a_n = \delta_{n,0}$ and $b_n = 0$. The probability amplitude for the particle to be transmitted into the n^{th} channel (propagating or not) on the right is c_n. For the propagating modes ($n \geq 0$), $c_n = t_{n,0}$. Using the above conditions into Eq.(2.9) we get a three term recursive relation for the coefficients c_n:

$$c_n + ih_n c_{n+1} + ih_{n-1} c_{n-1} = \delta_{n,0} \tag{2.18}$$

Let us now define the following quantity

$$f_n = \frac{c_n}{c_{n+1}} \qquad -\infty < n < \infty \tag{2.19}$$

In terms of f_n, Eq.(2.18) gives,

$$1 + \frac{ih_n}{f_n} + ih_{n-1} f_{n-1} = 0 \qquad \text{for } n \neq 0 \tag{2.20}$$

$$1 + \frac{ih_0}{f_0} + ih_{-1} f_{-1} = \frac{1}{c_0} \qquad \text{when } n=0. \tag{2.21}$$

For $n \geq 0$ we can write the solution of (2.20) in the form

$$f_n = \frac{1}{-ih_n}(1 + \frac{ih_{n+1}}{f_{n+1}}), \tag{2.22}$$

or,

$$f_n = \frac{1}{-ih_n}(1 + \cfrac{h_{n+1}^2}{1 + \cfrac{h_{n+2}^2}{1 + \cfrac{h_{n+3}^2}{\ddots}}}). \tag{2.23}$$

For $n \leq -1$ we write the solution in the form

$$f_n = \frac{-ih_n}{1 + ih_{n-1}f_{n-1}} \tag{2.24}$$

or,

$$f_n = \cfrac{-ih_n}{1 + \cfrac{h_{n-1}^2}{1 + \cfrac{h_{n-2}^2}{1 + \cfrac{h_{n-3}^2}{\ddots}}}}. \tag{2.25}$$

From the above expressions for the f_n's (when $n = 0$ and $n = -1$) we can obtain c_0 from Eq.(2.21),

$$c_0 = t_{0,0} = \frac{1}{1 + \frac{ih_0}{f_0} + ih_{-1}f_{-1}} = \cfrac{1}{1 + \cfrac{h_0^2}{1 + \cfrac{h_1^2}{1 + \cfrac{h_2^2}{1 + \cfrac{h_3^2}{\ddots}}}} + \cfrac{h_{-1}^2}{1 + \cfrac{h_{-2}^2}{1 + \cfrac{h_{-3}^2}{1 + \cfrac{h_{-4}^2}{\ddots}}}}} \tag{2.26}$$

With the solution for the $f_n's$ and c_0 known, any coefficient c_n can be found (using Eq.2.19) in the following way,

$$c_n = \frac{c_0}{f_{n-1}f_{n-2}\cdots f_0} \quad \text{for } n \geq 1$$

and

$$c_n = f_n f_{n+1} \ldots . f_{-1} c_0 \quad \text{for } n \leq -1 \tag{2.27}$$

From here, the transmission probability, T_0, can be written as

$$T_0 = \sum_{n=0}^{\infty} |c_n|^2 = |t_{0,0}|^2 (1 + \sum_{n=1} \frac{1}{\prod_{n'=1}^{n} |f_{n'-1}|^2}) = |t_{0,0}|^2 S(\varepsilon, V). \tag{2.28}$$

As it can be seen in Fig. 2.1, none of the $f_n's$ (for $n \geq 0$) appear to have zeros in the half-plane $\mathrm{Re}[\varepsilon] > 0$. This implies that the function $S(\varepsilon, V)$ has neither zeros nor poles in that region; consequently, the zeros and poles in the transmission probability are the zeros and poles of $|t_{0,0}|^2$. From now on we concentrate on $t_{0,0}$ only.

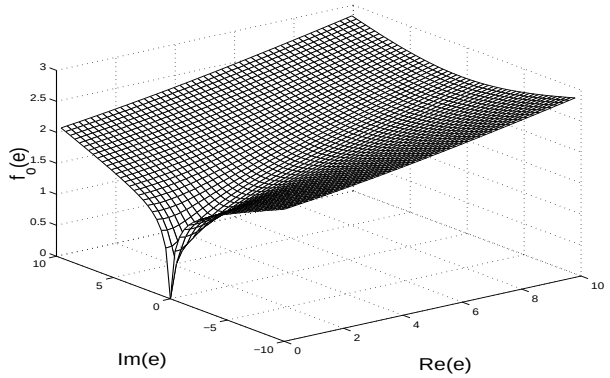

Figure 2.1: Graph of $|f_0(E)|^2$ in the complex plane (E in units of $\hbar\omega$). $a \equiv \frac{mV^2}{8\hbar^3\omega} = 10$. Notice that $f_n(\varepsilon) = f_0(n\hbar\omega + \varepsilon) = f_0(E)$. The function behaves similarly, but with a different scale, for other values of a.

2.4 Transmission Zeros

The coefficient c_0 can be taken to be a continuous function of the incoming energy $E = \varepsilon + n\hbar\omega$, instead of a function of the Floquet energy ε. This is so because, when the incident energy is in channel m ($E = m\hbar\omega + \varepsilon$), we need to solve Eq.(2.9) with the condition $a_n = \delta_{n,m}$. The solution is given in terms of the coefficient c_m which now plays the former role of c_0. The C.F. for c_m is given by Eq.(2.26) with m added to all subscripts. As it can be seen easily, $c_m(\varepsilon) = c_0(m\hbar\omega + \varepsilon) = c_0(E)$, which means that the general solution of the problem, for any incoming energy can be obtained from the C.F. expression for c_0 derived in Eq.(2.26) evaluating it at any energy E. Notice also that $c_0(E) = c_0(m\hbar\omega + \varepsilon) = t_{m,m}(\varepsilon)$. Because of this, and to be rigorous with the notation, we define $t_0(E) = t_0(m\hbar\omega + \varepsilon) \equiv t_{m,m}(\varepsilon) = c_0(E) = t_{0,0}(E)$. From this we can say that $t_0(E)$ contains the same information as the whole diagonal of the transmission matrix $\bar{t}$ in Eq.(2.14).

To study the properties of $c_0(E)$ it is convenient to define the following quantities (see Eq. 2.8)

$$g_n(\epsilon) \equiv {h_n}^2(\varepsilon) = \frac{a}{\sqrt{\epsilon + n}\sqrt{\epsilon + n + 1}}$$

with dimensionless parameters

$$a \equiv \frac{mV^2}{8\hbar^3\omega}, \qquad\qquad \epsilon \equiv \frac{\varepsilon}{\hbar\omega}$$

and

$$e \equiv \frac{E}{\hbar\omega} = \epsilon + n \quad \text{for} \quad n\hbar\omega \leq E \leq (n+1)\hbar\omega \tag{2.29}$$

Also, we define the function

$$F_0(e) = F_0(n+\epsilon) \equiv F_n(\epsilon) \equiv 1 + i\frac{h_0(n+\epsilon)}{f_0(n+\epsilon)} = 1 + \cfrac{g_n(\epsilon)}{1 + \cfrac{g_{n+1}(\epsilon)}{1 + \cfrac{g_{n+2}(\epsilon)}{\ddots}}} \tag{2.30}$$

Notice that $g_n(\epsilon)$ also depends on a.

Using the definitions given above we can write the coefficient $c_0(e)$ for the range $n \leq e \leq (n+1)$, in the following way

$$c_0(e) = c_0(n+\epsilon) = \cfrac{1}{F_n(\epsilon) + \cfrac{g_{n-1}(\epsilon)}{\ddots \cfrac{}{1 + \cfrac{g_0(\epsilon)}{1 + \cfrac{g_{-1}(\epsilon)}{1 + \cfrac{g_{-2}(\epsilon)}{\ddots}}}}}} \tag{2.31}$$

In the above expression all quantities are real (for ϵ real) except for $g_{-1}(\epsilon)$ which is pure imaginary. This has an important consequence for the number of real zeros in $c_0(e)$ as we shall see next.

Let us rewrite the equation above in a slightly different way:

$$c_0(n+\epsilon) = \cfrac{1}{F_n(\epsilon) + \cfrac{g_{n-1}(\epsilon)}{1 + \cfrac{g_{n-2}(\epsilon)}{\ddots \cfrac{}{1 + \cfrac{g_o(\epsilon)}{1 + iG(\epsilon)}}}}} \tag{2.32}$$

where the continued fraction $G(\epsilon)$ is defined as

$$G(\epsilon) \equiv \cfrac{-a}{\sqrt{1-\epsilon}\sqrt{\epsilon}(1+\cfrac{g_{-2}(\epsilon)}{1+\cfrac{g_{-3}(\epsilon)}{\ddots}})} \tag{2.33}$$

Notice $G(\epsilon)$ is a real function for ϵ real and $0 \leq \epsilon \leq 1$.

If Eq. (2.32) is put in the form of a standard fraction, we get

$$c_0(\epsilon) = \frac{1}{F_0 + iG} \qquad \text{for } n{=}0$$

and

$$c_0(n+\epsilon) = \frac{iP_n(g_{n-2}, g_{n-3}, ..., g_0)G + R_n(g_{n-2}, g_{n-3}..., g_0)}{iQ_n(F_n, g_{n-1}, ..., g_0)G + S_n(F_n, g_{n-1}, ..., g_0)} \qquad \text{for } n{>}0 \tag{2.34}$$

In the last expression, P_n, Q_n, R_n, S_n are polynomials on the variables g_n and F_n indicated in parentheses, such that the coefficient of every term is equal to one and all variables appear elevated to the first power only (i.e. $1 + g_1 + g_1 g_2 + ..$). Notice that G is the only function that can take values between $-\infty$ to ∞. The other functions (F_n and g_n) are strictly positive and finite for $\epsilon > 0$. This implies that P_n, Q_n, R_n, S_n are strictly positive and finite, which means that, for $n > 0$, the numerator of c_0 can never be zero and the denominator does not go to infinity unless $G \to \infty$, in which case the numerator would also blow up keeping the fraction strictly positive. From this we can conclude that *there are no real transmission zeros for incident energies $E > \hbar\omega$.*

For n=0 we see that a real zero can only happen when $F_0(\epsilon, a) \longrightarrow \infty$ or $G(\epsilon, a) \longrightarrow \infty$. The first case only occurs when $\epsilon = 0$ (G blows up at this

point too). For the second case, the real zeros of $t_0(\epsilon, a)$ are given by the zeros of $G^{-1}(\epsilon, a)$. As it can be seen from Fig. 2.2 the function $G^{-1}(\epsilon, a)$ seems to have some periodicity. This can also be seen in Fig. 2.3 where the curves $\delta(a)$ that satisfy $t_0(\delta, a) = G^{-1}(\delta, a) = 0$ are shown. This dependence of the transmission real zeros with the parameter a can be seen directly in Fig. 2.4 in the sequence of transmission graphs for different values of the strength of the delta.

It is interesting to notice in Fig. 2.3 and Fig. 2.4 that there are intervals of a, around integer values, for which the real zero in the transmission disappears. A table (for $0 \leq a \leq 9$) with the exact values (to seven digits) of the intervals for which there is a real zero in the transmission (apart from the trivial one at $E = 0$) is shown in Table 2.1. This behavior of the real zero seems to be matched by the behavior of the poles of the transmission as we will see next.

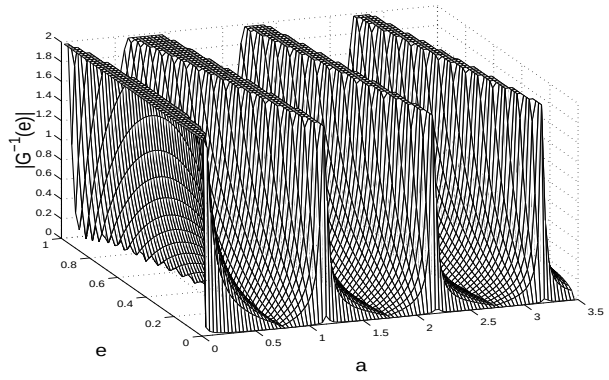

Figure 2.2: Graph of the function $|G^{-1}(\epsilon, a)|$. The zeros of this function give the real zeros of the transmission.

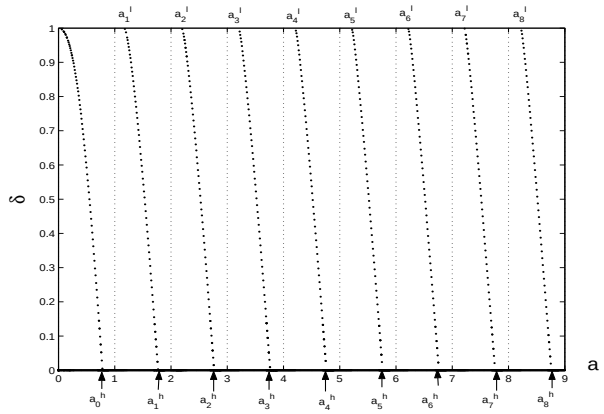

Figure 2.3: Location of the real zero of t_0 as a function of a.
$t_0(\delta, a) = G^{-1}(\delta, a) = 0$.

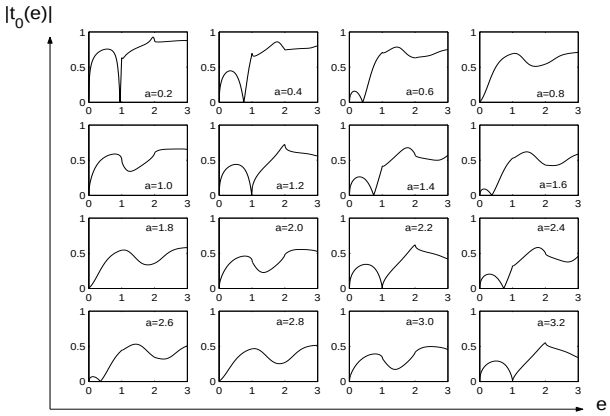

Figure 2.4: Sequence of $|t_0(e)|$ graphs for increasing values of a showing the evolution of the transmission real zeros.

	l	h
a_0	0	0.7821147
a_1	1.1652568	1.7710590
a_2	2.1873508	2.7667368
a_3	3.1979937	3.7642963
a_4	4.2045658	4.7626808
a_5	5.2091415	5.7615115
a_6	6.2125623	6.7606150
a_7	7.2152455	7.7598995
a_8	8.2174231	8.7593115

Table 2.1: Intervals of a=$\frac{mV^2}{8\hbar^3\omega}$ for which a zero-pole resonance can be found in the system. The notation a_n^l/a_n^h (used in the text and in some graphs) refers to the lower/higher value of the interval a_n.

2.5 Transmission Poles

In this section we prove by induction that the poles of $c_0(e)$ occur at energies $e = (n+\epsilon^*)$ with $0 < Re(\epsilon^*) < 1$ and show that their residue decreases with increasing n (energy). We start with equation (2.31) and write it in the form

$$c_0(n+\epsilon) = \frac{1}{F_n(\epsilon) + G_n(\epsilon)} \tag{2.35}$$

where F_n and G_n satisfy

$$F_n(\epsilon) = 1 + \frac{g_n(\epsilon)}{F_{n+1}(\epsilon)}$$

$$G_n(\epsilon) = \frac{g_{n-1}(\epsilon)}{1 + G_{n-1}(\epsilon)} \tag{2.36}$$

Let's assume that $c_0(e)$ has a pole at $e = n + \epsilon^*$. This implies that $c_0(e)$ has also a pole at $e = n + 1 + \epsilon^*$ because we can write from Eqs. (2.35) and (2.36)

$$\begin{aligned} c_0(n+1+\epsilon) &= \frac{1}{F_{n+1}(\epsilon) + G_{n+1}(\epsilon)} \\ &= \frac{1}{\dfrac{g_n(\varepsilon)}{F_n(\epsilon) - 1} + \dfrac{g_n(\epsilon)}{1 + G_n(\epsilon)}} \\ &= \frac{(1 + G_n(\epsilon))(F_n(\epsilon) - 1)}{g_n(\epsilon)(F_n(\epsilon) + G_n(\epsilon))} \\ &= \frac{(1 + G_n(\epsilon))}{F_{n+1}(\epsilon)(F_n(\epsilon) + G_n(\epsilon))} \end{aligned} \tag{2.37}$$

It is important to notice that, since $f_0(e)$ (as shown in Fig.2.1) has neither poles nor zeros in the half plane $Re(e) > 0$, the function $F_n(\epsilon) = F_0(n+\epsilon) = 1 + i\frac{h_0(e)}{f_0(e)}$ does not have poles and $F_n(\epsilon) \neq 1$. This implies that (from the last line of Eq. (2.37)) if $c_0(e)$ has a pole at $n+\epsilon^*$ (which means that $F_n(\epsilon^*)+G_n(\epsilon^*) = 0$), then it must have a pole at $n + 1 + \epsilon^*$ (The numerator in Eq. (2.37) does not vanish at $\epsilon = \epsilon^*$ because $G_n(\epsilon^*) = -F_n(\epsilon^*) \neq -1$).

Notice also that when $n \longrightarrow \infty$, $F_n \longrightarrow 1$, because $f_0(n+\epsilon) \to \infty$, and $h_0(n + \epsilon) \to 0$ in this limit. This means that the location of the transmission zero approaches the location of the pole as the incoming energy grows; the zero happens when $\epsilon = \delta$, with $G_n(\delta) = -1$; the pole occurs when $\epsilon = \epsilon^*$, with $G_n(\epsilon^*) = -F_n(\epsilon^*)$. Obviously $\delta \to \epsilon^*$ because $F_n(\epsilon^*) \longrightarrow 1$ as $n \to \infty$. From that we conclude that the residue of the poles in the transmission amplitude tend to zero as $n \longrightarrow \infty$. This explains why, even though the transmission amplitude has an infinite number of poles separated by a distance of $\hbar\omega$ in the

incoming energy, all at the same distance from the real axis, only the effect of the first poles can be seen in the graphs of transmission probability versus incoming energy. Another way to say this is that the zeros (in the complex plane) at higher energies are very close to the poles, therefore cancelling out the possible effect of the poles in the transmission.

In Fig. 2.5 we show a graph of the imaginary part of $t_0(e)$ where the poles in channels 0, 1, 2, can be seen (we refer to channel n as the strip in the complex energy plane that satisfies $n < Re(e) < n + 1$). It is evident in that graph that the poles have support on different sheets; we will call these sheets S_n, where n refers to the channel number. This sheeted structure comes from the fact that, because the functions $k_n(e)$ have a branch point at $e = -n$ and two Riemann sheets, any function of $k_n(e)$ ($t_0(e)$ in particular) will have a multiple-sheeted structure. What is called the "physical" sheet (P) in the context of multiple channel scattering is the sheet obtained when selecting all the Riemann sheets with $\mathrm{Im}(k_n) > 0$. Each sheet of the full multi-sheeted surface can be labelled by the sequence of signs of $\mathrm{Im}(k_\infty)$,..., $\mathrm{Im}(k_1)$, $\mathrm{Im}(k_0)$, $\mathrm{Im}(k_{-1})$,..., $\mathrm{Im}(k_{-\infty})$., e.g., $(+..-\mathbf{+}+..+)$ (bold has been used to indicate the sign of $\mathrm{Im}(k_0)$); fortunately we do not need to consider all these sheets, since only a small fraction of them are of physical interest; the principal one being P or $(+..+\mathbf{+}+..+)$. Crossing the real axis from P at an energy $m < e < m+1$ crosses all the branch cuts whose branch point is at an energy smaller than $e = m$ (see figure 2.6) . The sheet that is the smooth continuation of P into the lower complex plane (smooth even at the cut) is the one obtained by

taking $\mathrm{Im}(k_{-n})< 0$ for all $n \leq m$ and $\mathrm{Im}(k_{-n})> 0$ for all $n > m$. We call these sheets S_m and they are precisely the ones where the poles in the transmission are found, as shown schematically in Fig. 2.7.

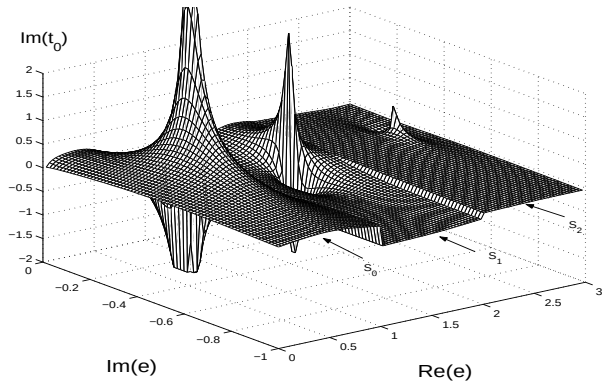

Figure 2.5: Graph of the imaginary part of $t_0(e)$ for a=0.5, showing several poles. Each pole is located on a different sheet.

Resonances, as opposed to bound state poles, do not occur in the "physical" sheet; however, from the unitarity of the S-matrix extended to the complex plane, they can have important effects on the behavior of the S-matrix along the real axis (see [25] for an excellent discussion on multiple channel scattering).

In single channel scattering, the unitarity of the S-matrix on the real axis has consequences in the analytic structure of the S-matrix in both sheets, the most important one being the zero-pole structure of the resonances: every pole has a companion zero at a position complex conjugate to the position of the pole but on a different sheet. For multiple channel scattering the position of the pole and zero are not so simply related and often the pole and zero

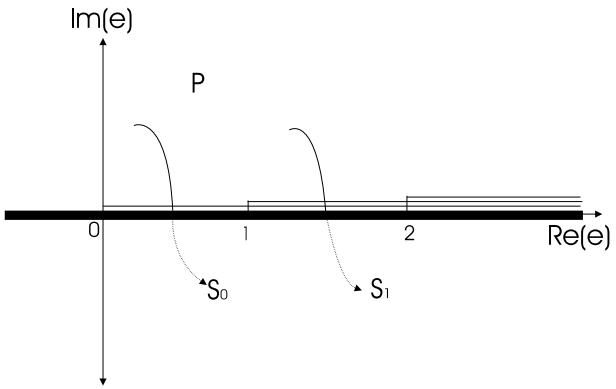

Figure 2.6: Top view of the physical sheet P and the threshold branch points and cuts in the complex energy plane. Indicated with a thin line are the branch cuts corresponding to the branch points $n = 0, 1, 2$; the thick line represents all the branch cuts with branch point at negative energy($n < 0$ branch points). Paths that start on the upper half of P and go under the branch cut lead to the different sheets S_n (which in this figure are assumed to be underneath P).

appear in the same sheet.

The position of the pole (e^*) in the first channel, can be found by looking at the zeros of the function $F_0(e, a) + G_0(e, a)$ with the appropriate selection of Riemann sheets, as described before, so as to be on the sheet S_0. A graph of the position of the pole as the strength of the potential is varied is shown in Fig. 2.8, where it can be seen that the pole approaches the real axis at $e^* = 1$ when $a \to 0$, annihilating the real zero which also goes to the same position with $a \to 0$. As the parameter a is increased the zero moves to the left on the real axis (see Fig. 2.3) and the pole moves away from the real axis describing an arch. At $a = a_0^h = 0.7821147$ (all values of a are accurate to the seventh digit) the zero disappears at $\delta = 0$ and so does the pole. For values of a slightly greater, the transmission has a very high peak but it is not a pole, as

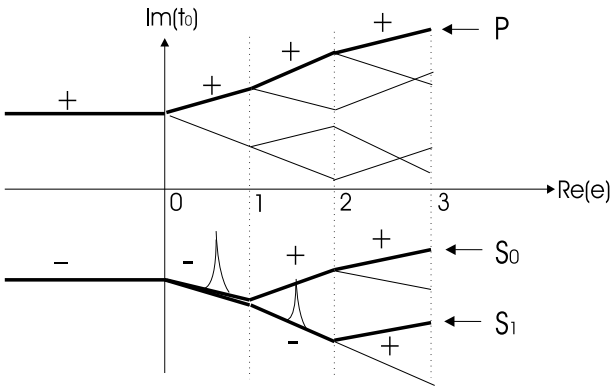

Figure 2.7: Sketch of $Im(t_0(e))$ versus $Re(e)$ (we assume $Im(e) = constant < 0$) which gives a schematic representation of the different sheets where the poles of the transmission are located. The peak structures in the lower part of the figure represent poles.

can be seen in Fig. 2.9 (compare with the pole at $a = 0.78$ in Fig. 2.10). In the interval $a_0^h < a < a_1^l$ the transmission does not have any zero-pole resonances. In this interval the peak or false "pole" follows a trajectory that seems the continuation of the trajectory the pole had followed until it vanished. When $a = a_1^l$ the zero reappears on this channel, entering at $\delta = 1$. At this value however, we do not see any pole in this channel. There is in fact a pole on S_0 but it is located in the next channel ($1 < Re(e^*) < 2$). For $a \approx 1.3$ the pole has finally made it into the $n = 0$ channel. As a is further increased the pole continues to describe an arch until it disappears along with the zero. A similar behavior to the one described above occurs for increasing values of the parameter a, with the pole describing ever increasing arches, each one farther away from the real axis than the previous one. An identical behavior of the poles on other sheets is expected from the discussion following Eq.(2.37).

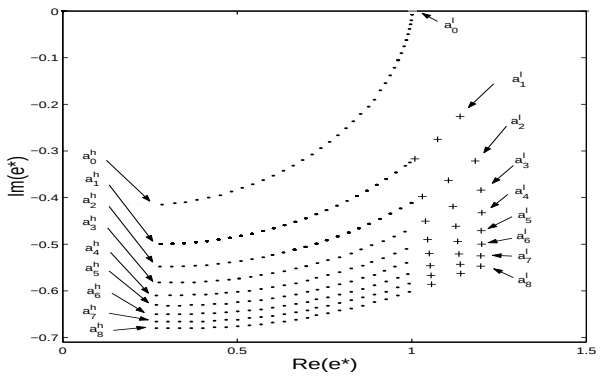

Figure 2.8: Trajectory of one of the transmission poles as a is changed from 0 to 9. Here a_n^l/a_n^h refers to the lower/higher value of the interval a_n given in Table 1.

The study of the behavior of the poles and real zeros as a function of the parameter $a = \frac{mV^2}{8\hbar^3\omega}$ shows an interesting quasi-periodic dependence on a and the presence of "bands" of non-resonant values of a for which the transmission does not have zero-pole resonances. This quasi-periodic behavior of the transmission resonances as a function of the strength of the oscillating potential and the driving frequency has not been found before. Around integer values of a the oscillating potential seems to be incapable of dynamically trapping particles not even for a short period of time. It can also be mentioned that the life-time of the quasi-bound states decreases with increasing a, which can be accomplished by either increasing the strength V of the potential or by decreasing the frequency of the oscillations.

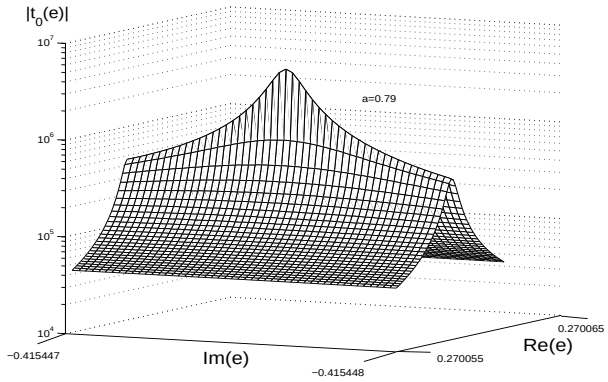

Figure 2.9: False "pole" of $t_0(e)$ for $a = 0.79$, right after the zero has disappeared at $\delta = 0$ for $a = a_0^h$.

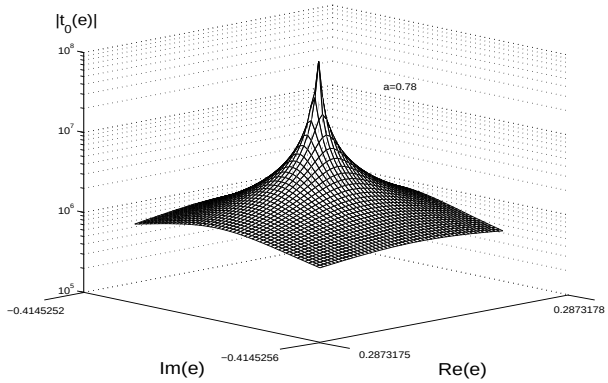

Figure 2.10: True pole of the transmission for $a = 0.78$, slightly lower than the value of a ($a = a_0^h$) for which the zero disappears.

2.6 Threshold anomalies

One of the most evident features in the transmission versus energy curves for all values of a is what seems to be a discontinuity in the slope at $e = n\hbar\omega$ (channel openings). A close look into this regions reveals that there is a rapid divergence of the slope at the thresholds, that is, $\frac{dt_0}{de} \to \pm\infty$ as $e \to n\hbar\omega$. This is actually a common occurrence in all multi-channel

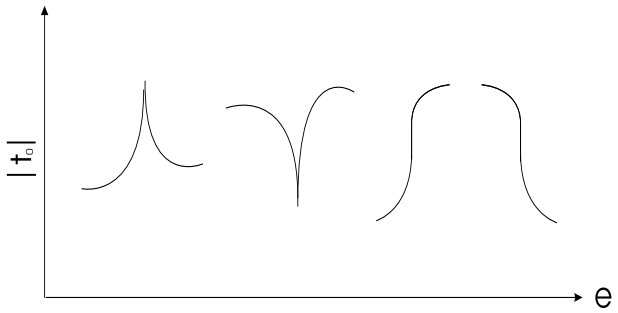

Figure 2.11: Various forms of transmission amplitude behavior at a channel opening.

scattering problems, and it can be traced back to the fact that when the energy is in the n^{th} channel near threshold, the first open-channel momentum is $k_{-n} = \sqrt{e - n\hbar\omega}$. It can be proven that the S-matrix has elements that are linear functions of this momentum near threshold. This clearly implies that the derivative of these elements with respect to the energy must diverge at threshold (for more details see [28]). These threshold anomalies can easily be proven to exist in our particular time dependent potential by looking at our C.F. solution for $c_0(e)$ in Eq. 2.31. From it, it is clear that the derivative of this expression gives an infinite number of terms, each one proportional to the derivative of some function $g_n(e)$. These functions and their derivatives diverge at their thresholds (see the expression for g_n in Eq. 2.29), therefore the derivative of $c_0(e)$ must also diverge at each threshold. According to this, the shape of the threshold anomaly can be of four different kinds, two cusps like and two rounded steps, as shown in Fig. 2.11. These four different kinds of anomalies are shown in Fig. 2.12 as they occur in the $|t_0(e)|$ graphs for two different values of a.

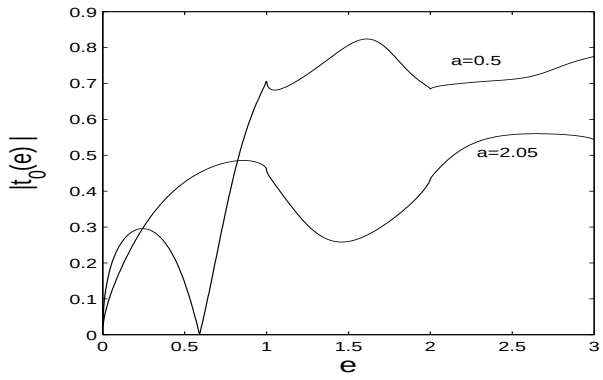

Figure 2.12: Graph of $|t_0(e)|$ vs. incoming energy. Threshold anomalies of "cusp" type at the channel openings for a=0.5 . Threshold anomalies of "rounded step" type for a=2.05 .

Chapter 3

Quasi-energy band structure of the harmonically driven δ-function chain

3.1 Introduction

In this chapter we study a time dependent potential which is space-time harmonic, that is, harmonic in its space and in its time dependence. In the last chapter we studied in detail a delta-function potential whose strength changed harmonically with time; in this chapter we will use some of the equations derived for the one-delta case and from them construct the solution for an infinite periodic chain of these oscillating delta functions.

Since the 1930s, the study of space-periodic potentials has yielded fundamental information about the properties of electrons in crystals. Tunnelling and interference effects give rise to the well known energy band structure in such materials. For real crystals, in addition to the band structure, one has to consider the interaction of the electrons with impurities or defects, the electron-electron interaction, and the electron-phonon interaction to give and accurate description of the dynamics of electrons in such materials.

The development of super-lattices and the more recent advances in atom optics have brought to the forefront the study of space periodic potentials

since, for the first time, it has been possible to observe fundamental quantum effects, due solely to the spatial periodicity of the potential, that had been predicted long ago. These include Landau-Zener tunnelling, Wannier-stark ladders, and Bloch oscillations, which occur in a periodic system driven by a D.C. electric field.[29]

The effects of time-periodic forces on spatially periodic systems have also been studied and interesting phenomena have been predicted (and some observed experimentally) such as dynamical localization (mini-band collapse)[30, 31], photon-assisted tunnelling [32], quantum hamiltonian ratchets [33, 34], chaos-assisted tunnelling [35–39], dynamic Anderson-localization [15] and quantization of particle transport[40].

Because of the myriad of phenomena that have been associated with space-time periodic potentials, it is interesting to study one of the simplest potentials which has both periodicities: a spatially periodic chain of δ-function potentials whose strength oscillates periodically in time. The mathematical simplicity of this potential permits an analytic computation of its eigenstates and eigenvalues with the use of continued fractions. This simplicity also allows for a clear understanding of the basic dynamical properties of a quantum particle under a space-time periodic potential. This system is special because its classical analog is quasi-integrable [41], whereas most other systems of this type are non-integrable.

In Section 3.2 we derive the Floquet-Bloch (FB) Hamiltonian for the oscillating delta chain and use it to investigate the quasi-energy (Q.E.) band

structure in the perturbative regime. In Section 3.3 we construct the Floquet translation matrix (TM). In Section 3.4, we solve for the eigenvalues and eigenvectors of the TM matrix using continued fractions. In Section 3.5, we study the structure of the eigenvectors in the negative energy channels and relate it to some scattering properties of the single δ-function potential which are derived in appendices A and B. In Section 3.6, we study how the Q.E. band structure changes as a function of the strength of the oscillating potential.

3.2 Floquet-Bloch approach

The Hamiltonian we will study in this paper is of the form (in the position representation),

$$H(x,t) = \frac{\hbar^2}{2\mu}\frac{\partial^2}{\partial x^2} + (\tilde{V}_0 + \tilde{V}_1 cos(\omega t)) \sum_{m=-\infty}^{\infty} \delta(x - mL) \tag{3.1}$$

Here x is the position, μ is the effective mass of the particle, $\tilde{V}_0$ is the strength of the static part of the potential, $\tilde{V}_1$ is the strength of the oscillating part of the potential, ω is the frequency of the oscillation, t is the time, and L is the distance between neighboring delta functions.

Since a wave function that satisfies Schrödinger's equation $i\hbar\frac{\partial\Psi}{\partial t} = H\Psi$ with Hamiltonian (1) must be quasi-periodic in time and space (Floquet-Bloch theorem), the solutions are of the form

$$\Psi_{\epsilon,\kappa}(x,t) = e^{-i\epsilon t/\hbar} e^{i\kappa x} \sum_{n=-\infty}^{\infty} \sum_{m=-\infty}^{\infty} \psi_{n,m} e^{2\pi m i \frac{x}{L}} e^{-in\omega t}, \tag{3.2}$$

where $\hbar$ is Planck's constant, $\psi_{n,m}$ is a probability amplitude, ϵ is the quasi-energy (with allowed values $0 \leq \epsilon \leq \hbar\omega$), and κ is the Bloch momentum (for which the first Brillouin zone is taken to be $-\pi/L \leq \kappa \leq \pi/L$). If we substitute the state $\Psi_{\epsilon,\kappa}(x,t)$, into the Schrodinger equation and use the fact that $\frac{1}{L}\int_{-L/2}^{L/2} dx\, \exp(\frac{2\pi i}{L}(m-m')x) = \delta_{m,m'}$ and $\frac{1}{T}\int_o^T dt\, \exp(i\omega(n-n')t) = \delta_{n,n'}$, we obtain an eigenvalue equation for the amplitude $\psi_{n,m}$

$$\sum_{n'=-\infty}^{\infty}\sum_{m'=-\infty}^{\infty} \tilde{H}^{FB}_{n,n',m,m'}\psi_{n',m'} = \epsilon\ \psi_{n,m} \tag{3.3}$$

where $\tilde{H}^{FB}$ is the FB Hamiltonian matrix

$$\tilde{H}^{FB}_{n,n',m,m'} = \left(\frac{\hbar^2}{2\mu}(\kappa + \frac{2\pi}{L}m)^2 - n\hbar\omega\right)\delta_{n,n'}\delta_{m,m'} + \frac{\tilde{V}_0}{L}\delta_{n,n'} + \frac{\tilde{V}_1}{2L}(\delta_{n-1,n'} + \delta_{n+1,n'}). \tag{3.4}$$

Diagonalization of this matrix yields the quasi-energies and eigenvectors as a function of the Bloch-momentum κ.

For computational purposes, it is convenient to define the following dimensionless quantities,

$$\begin{aligned} \varepsilon \equiv \epsilon/\hbar\omega, \quad l_\omega = \sqrt{\frac{\hbar}{2\mu\omega}} \quad l \equiv L/l_\omega, \quad k \equiv \kappa l_\omega, \quad x' \equiv x/l_\omega, \\ V_1 \equiv \frac{\mu\tilde{V}_1 l_\omega}{2\hbar^2}, \quad V_0 \equiv \frac{\mu\tilde{V}_0 l_\omega}{\hbar^2}, \quad H^{FB} \equiv \tilde{H}^{FB}/\hbar\omega. \end{aligned} \tag{3.5}$$

Notice that l_ω is the wavelength of a particle with effective mass μ and energy $\hbar\omega$. In terms of these dimensionless variables, the FB Hamiltonian takes the form

$$H^{FB}_{n,n',m,m'} = \left(\frac{1}{l^2}(kl + 2\pi m)^2 - n\right)\delta_{n,n'}\delta_{m,m'} + 2\frac{V_0}{l}\delta_{n,n'} + 2\frac{V_1}{l}(\delta_{n-1,n'} + \delta_{n+1,n'}) \tag{3.6}$$

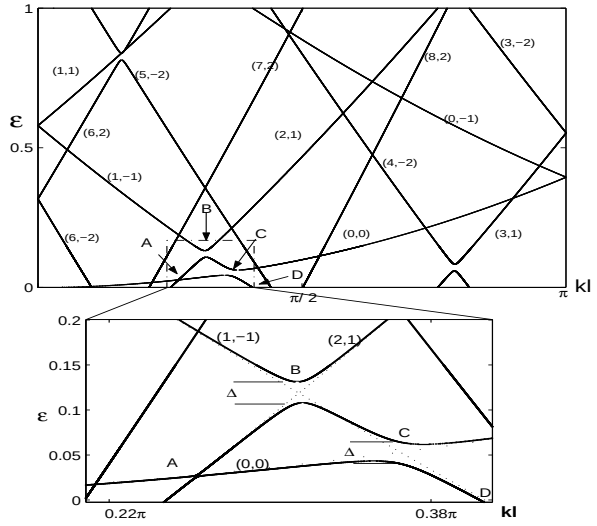

Figure 3.1: Quasi-energy curves for $V_0 = 0$, $V_1 = 0.03$, $l = 5$. Curves have been labelled using (n,m) pairs, where the energy of the corresponding unperturbed state is $E = (n + \varepsilon)\hbar\omega$, and its wave vector is $K = k + 2\pi m/l$. Features A, B, C, and D are indicated. The inset shows a magnification of the dashed box.

For zero static potential, $V_0 = 0$, and small V_1, the quasi-energy bands can be labelled away from the avoided crossings, by the integer pair (n, m) as is shown in Fig.3.1 for the parameters $V_1 = 0.03,\ l = 5$. The FB eigenvector corresponding to the point $\varepsilon_{(n,m)}(kl)$ on band (n,m), is a plane wave with (dimensionless) energy $E = (n + \varepsilon)$ and (dimensionless) momentum $K = k + \frac{2\pi}{l}m$. The curve in Fig.3.1 for the pair (n, m) is obtained by drawing a parabola centered at the point (n, 2πm) in the infinite plane (E, K). The

segment of the parabola that crosses the region $0 \leq E \leq 1$, $-\pi/l < K \leq \pi/l$, gives rise to the quasi-energy band labelled (n, m).

It is also useful to plot the average energy of the FB eigenstates, $\Psi_{\epsilon,\kappa}(x,t)$, which we define as,

$$< E > \equiv \sum_n (\varepsilon + n) \sum_m |\psi_{n,m}|^2 \quad , \tag{3.7}$$

This is shown in Fig.3.2 for the same parameters chosen for Fig. 3.1. Let us focus on three features, marked A,B,C, in Fig. 3.1 and 3.2. We begin by studying B, an avoided crossing between bands (1,-1) and (2,1). From first order degenerate perturbation theory we obtain the reduced 2x2 Hamiltonian near the point $kl \sim 1$:

$$H^{FB} = \begin{bmatrix} \varepsilon^0_{1,-1}(kl) & 2\frac{V_1}{l} \\ 2\frac{V_1}{l} & \varepsilon^0_{2,1}(kl) \end{bmatrix} \tag{3.8}$$

where the unperturbed quasi-energies are:

$\varepsilon^0_{1,-1}(kl) = \frac{1}{25}(kl - 2\pi)^2 - 1$ and $\varepsilon^0_{2,1}(kl) = \frac{1}{25}(kl + 2\pi)^2 - 2$

The eigenvalues of this Hamiltonian matrix give the quasi-energy bands in the neighborhood of the crossing,

$$\varepsilon^{\pm}(kl) = \frac{1}{2}\left(\varepsilon^0_{1,-1}(kl) + \varepsilon^0_{2,1}(kl)\right) \pm \frac{1}{2}\sqrt{\left(\varepsilon^0_{1,-1}(kl) - \varepsilon^0_{2,1}(kl)\right)^2 + 16\left(\frac{V_1}{l}\right)^2} \tag{3.9}$$

At the middle of the avoided crossing, where $\varepsilon^0_{1,-1} = \varepsilon^0_{2,1}$, the distance between the bands, Δ, is

$$\Delta = 4\frac{V_1}{l} \tag{3.10}$$

Note that the width of the avoided crossing does not depend on the energy or momentum of the bands involved, which is a peculiar feature of the delta-function chain. Therefore, for the delta-function chain, all first-order avoided crossings have the same width, Δ.

Feature C is an example of a first order avoided crossing between bands (0,0) and (1,-1). Note that the first order avoided crossings in the quasi-energy plot reveal themselves as crossings in the average energy plot. This happens because at an avoided crossing the two states exchange identities, and the average energy includes the contribution from both states.

Feature A, in Fig. 3.2, is a second order avoided crossing, involving a two phonon process between the unperturbed states (2,1) and (0,0). This is evident in Fig. 3.2, where the crossing occurs between a band with average energy near $2\hbar\omega$ and a band near 0 $\hbar\omega$.

Feature D in Fig. 3.2 can not be explained using degenerate perturbation theory. It is not the result of an avoided crossing between unperturbed states. This feature occurs when the unperturbed quasi-energy band (1,-1) (in Fig. 3.1) crosses the lower edge of the quasi-energy Brillouin zone ($\varepsilon = 0$). This sudden drop in the average energy of the eigenstate will be discussed later.

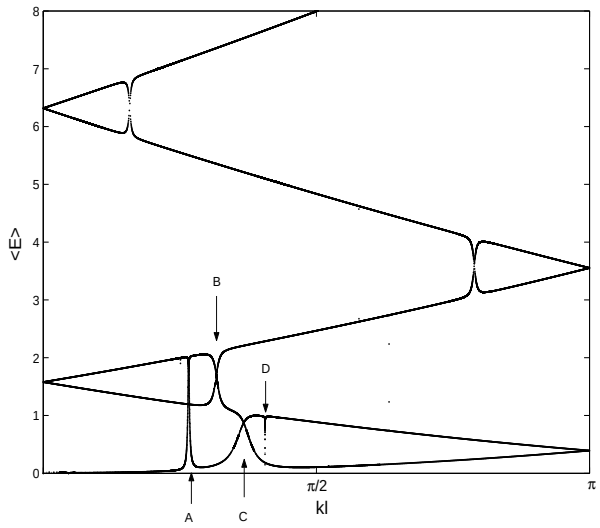

Figure 3.2: Average energy, $\langle E \rangle$, versus Bloch momentum, k, for $V_0 = 0$,$V_1 = 0.03$,$l = 5$. Features A, B, C, and D (discussed in the text) are indicated.

3.3 Translation Matrix

Let us now construct the Floquet translation matrix for the δ-function chain. This will be done in two steps. First, we calculate the transfer matrix connecting the Floquet-coefficients of the wave-function (Eq. 3.2) on the left and on the right of a δ-function. Then we calculate the translation matrix which connects the Floquet-components of the wave function on the left side of a delta-function with the components on the left side of the nearest neighbor delta-function. The eigenvectors of this translation matrix will have either pure real (norm of eigenvalue equal to one) or complex (norm different from one) Bloch-momentum. The cases with real Bloch-momentum correspond to the physical states, while the eigenfunctions with complex Bloch momentum are not physical since they diverge in one direction along the x-axis.

3.3.1 Time Periodicity

Let us write the FB state, $\Psi_{\epsilon,\kappa}(x,t)$, in terms of dimensionless variables, and in the form

$$\Psi_{\varepsilon}(x',\tau) = \sum_{n=-\infty}^{\infty} \psi_n(x') e^{-i(\varepsilon+n)\tau}. \tag{3.11}$$

where $\psi_n(x')$ contains all the spatial dependance of the wave-function. Since the potential is zero everywhere except at $x' = ml$, we assume $\psi_n(x')$ in regions I and II (on the left and right of the δ-function at $x' = 0$, respectively) to be of the form

$$\begin{aligned} {\psi_n}^{I}(x') &= \frac{1}{\sqrt{k_n}}(a_n e^{ik_n x'} + d_n e^{-ik_n x'}) \quad \text{for } -l < x < 0 \\ {\psi_n}^{II}(x') &= \frac{1}{\sqrt{k_n}}(c_n e^{ik_n x'} + b_n e^{-ik_n x'}) \quad \text{for } 0 < x < l. \end{aligned} \tag{3.12}$$

For finite chains, the factor $\frac{1}{\sqrt{k_n}}$ is included to ensure unitarity of the S-matrix[42]; we also use that convention here. The dimensionless wave-vectors, k_n, are given by

$$k_n \equiv \sqrt{\varepsilon + n}. \tag{3.13}$$

Note that for $n < 0$ the wave vector is imaginary and gives rise to exponentially decaying and growing modes. These will be discussed later.

Continuity of $\Psi_{\varepsilon}(x',\tau)$ at $x' = 0$ gives

$$a_n + d_n = c_n + b_n. \tag{3.14}$$

Because of the delta function in the Hamiltonian, the spatial derivative of

$\Psi_\varepsilon(x',\tau)$ at $x'=0$ is discontinuous and satisfies

$$\left.\frac{d\Psi_\varepsilon}{dx'}\right|_{x'=0^+} - \left.\frac{d\Psi_\varepsilon}{dx'}\right|_{x'=0^-} = [V_0 + V_1\cos(\tau)]\Psi_\varepsilon(0,\tau). \tag{3.15}$$

This leads to the condition

$$c_n+d_n-b_n-a_n = -2i\,[s_n(a_n+d_n)+h_{n-1}(a_{n-1}+d_{n-1})+h_n(a_{n+1}+d_{n+1})], \tag{3.16}$$

where,

$$h_n = \frac{V_1}{(\varepsilon+n)^{1/4}(\varepsilon+n+1)^{1/4}} \quad \text{and} \quad s_n = \frac{V_0}{\sqrt{\varepsilon+n}}. \tag{3.17}$$

Using (3.14) and (3.16) we solve for c_n and b_n in terms of a_n and d_n to obtain,

$$c_n = a_n - is_na_n - ih_{n-1}a_{n-1} - ih_na_{n+1} - is_nd_n - ih_{n-1}d_{n-1} - ih_nd_{n+1} \tag{3.18}$$

and

$$b_n = d_n + is_na_n + ih_{n-1}a_{n-1} + ih_na_{n+1} + is_nd_n + ih_{n-1}d_{n-1} + ih_nd_{n+1} \tag{3.19}$$

It is useful to define the column vectors $\mathbf{A}$, $\mathbf{B}$, $\mathbf{C}$, and $\mathbf{D}$ with components a_n, b_n, c_n, and d_n, respectively. Then Eqs. (3.18) and (3.19) can be written in matrix form as

$$\mathbf{C} = (\mathbf{1}-\mathbf{X})\cdot\mathbf{A} - \mathbf{X}\cdot\mathbf{D} \tag{3.20}$$

$$\mathbf{B} = \mathbf{X}\cdot\mathbf{A} + (\mathbf{1}+\mathbf{X})\cdot\mathbf{D} \tag{3.21}$$

where the matrix $\mathbf{X}$ has components

$$[X]_{n,n'} = \delta_{n',n-1}ih_{n'} + \delta_{n',n+1}ih_{n'-1} + \delta_{n',n}is_n. \tag{3.22}$$

This system of equations can also be written as

$$\begin{pmatrix} \mathbf{C} \\ \mathbf{B} \end{pmatrix} = \mathbf{M} \cdot \begin{pmatrix} \mathbf{A} \\ \mathbf{D} \end{pmatrix} \tag{3.23}$$

with

$$\mathbf{M} = \begin{bmatrix} \mathbf{1} - \mathbf{X} & -\mathbf{X} \\ \mathbf{X} & \mathbf{1} + \mathbf{X} \end{bmatrix} \tag{3.24}$$

The matrix M relates components of the eigenstates on opposite sides of a single δ-function in the infinite chain.

3.3.2 Spatial Periodicity

Because of the spatial periodicity of the Hamiltonian Eq. (3.1), Floquet-Bloch states have the property

$$\mathcal{T}^l \Psi_{\varepsilon,k}(x') = \Psi_{\varepsilon,k}(x' + l) = \lambda \Psi_{\varepsilon,k}(x'), \tag{3.25}$$

where $\mathcal{T}^l$ is the translation by l operator and λ is its eigenvalue, which satisfies $\lambda = e^{ikl}$ for k real (Bloch momentum) when $\Psi_{\varepsilon,k}(x')$ is a Bloch-function. Imposing this condition on the wave function and its derivative at the point $x' = -l/2$, we obtain

$$\begin{aligned} \lambda(a_n e^{-ik_n l/2} + d_n e^{ik_n l/2}) &= c_n e^{ik_n l2} + b_n e^{-ik_n l/2} \\ \lambda(a_n e^{-ik_n l/2} - d_n e^{ik_n l/2}) &= c_n e^{ik_n l/2} - b_n e^{-ik_n l/2} \ . \end{aligned} \tag{3.26}$$

We can write this set of equations as,

$$\lambda \begin{bmatrix} \mathbf{T}_{-l/2} & \mathbf{T}_{l/2} \\ \mathbf{T}_{-l/2} & -\mathbf{T}_{l/2} \end{bmatrix} \begin{pmatrix} \mathbf{A} \\ \mathbf{D} \end{pmatrix} = \begin{bmatrix} \mathbf{T}_{l/2} & \mathbf{T}_{-l/2} \\ \mathbf{T}_{l/2} & -\mathbf{T}_{-l/2} \end{bmatrix} \begin{pmatrix} \mathbf{C} \\ \mathbf{B} \end{pmatrix}, \tag{3.27}$$

where the matrix $T_{\pm l/2}$ is diagonal and has matrix elements $e^{\pm ik_n l/2}$. We can now write

$$\begin{aligned}\lambda\begin{pmatrix}\mathbf{A}\\ \mathbf{D}\end{pmatrix} &= \begin{bmatrix}\mathbf{T}_{-l/2} & \mathbf{T}_{l/2}\\ \mathbf{T}_{-l/2} & -\mathbf{T}_{l/2}\end{bmatrix}^{-1}\begin{bmatrix}\mathbf{T}_{l/2} & \mathbf{T}_{-l/2}\\ \mathbf{T}_{l/2} & -\mathbf{T}_{-l/2}\end{bmatrix}\begin{pmatrix}\mathbf{C}\\ \mathbf{B}\end{pmatrix}\\ &= \frac{1}{2}\begin{bmatrix}\mathbf{T}_{l/2} & \mathbf{T}_{l/2}\\ \mathbf{T}_{-l/2} & -\mathbf{T}_{-l/2}\end{bmatrix}\begin{bmatrix}\mathbf{T}_{l/2} & \mathbf{T}_{-l/2}\\ \mathbf{T}_{l/2} & -\mathbf{T}_{-l/2}\end{bmatrix}\begin{pmatrix}\mathbf{C}\\ \mathbf{B}\end{pmatrix}\\ &= \begin{bmatrix}\mathbf{T}_{l} & \mathbf{0}\\ \mathbf{0} & \mathbf{T}_{-l}\end{bmatrix}\begin{pmatrix}\mathbf{C}\\ \mathbf{B}\end{pmatrix}\end{aligned} \tag{3.28}$$

If combine Eqs. (3.23), (3.24), and (3.28), we obtain

$$\mathbf{TM}\begin{pmatrix}\mathbf{A}\\ \mathbf{D}\end{pmatrix} = \lambda\begin{pmatrix}\mathbf{A}\\ \mathbf{D}\end{pmatrix} \tag{3.29}$$

where

$$\mathbf{TM} = \begin{bmatrix}\mathbf{T}_{l}(\mathbf{1}-\mathbf{X}) & -\mathbf{T}_{l}\mathbf{X}\\ \mathbf{T}_{-l}\mathbf{X} & \mathbf{T}_{-l}(\mathbf{1}+\mathbf{X})\end{bmatrix} \tag{3.30}$$

is the Floquet translation matrix. After diagonalizing the TM matrix, one selects the eigenvectors corresponding to eigenvalues $|\lambda| = 1$. These are the Floquet-Bloch states of the system.

3.3.3 Static Potential Case ($V_0 \neq 0, V_1 = 0$)

For a purely static potential, the TM matrix is a 2x2 matrix with two distinct eigenvalues and corresponding eigenvectors. It can be shown that,

$$TM = \begin{bmatrix}e^{ikl}(1+\frac{Vo}{2ik}) & e^{ikl}(\frac{Vo}{2ik})\\ e^{-ikl}(-\frac{Vo}{2ik}) & e^{-ikl}(1-\frac{Vo}{2ik})\end{bmatrix}, \tag{3.31}$$

where $k = \sqrt{2E}$.

A graph of the absolute value of the two eigenvalues of TM, as a function of energy, for the static delta chain is shown in Fig. 3.3a. The prohibited

energy regions are the regions occupied by the "bubbles." These occur at energies for which the absolute value of the eigenvalues of TM is not one. The well-known band structure for this potential is obtained by plotting energy vs. Bloch momentum as shown in Fig. 3.3b. For the parameters chosen in Fig.3.3, the delta-function potential has a bound state at $E = -1$. That is precisely the location of the negative energy band, which occupies the region $-1.025 < E < -0.975$ in units of the bound state energy $|E_{bound}| = \frac{V_o^2}{2}$. The width of this band is known to decrease rapidly with the distance between wells [47]. For $l = 5$ it is already of the order of 10^{-3}.

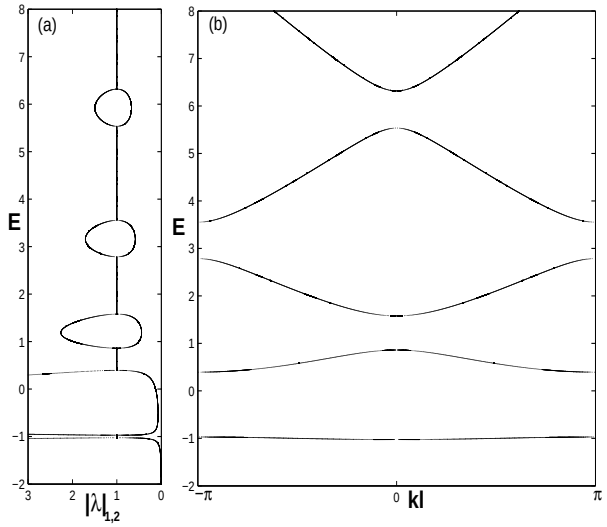

Figure 3.3: (a)Energy, E, plotted as a function of the absolute value of eigenvalues $\lambda_{1,2}$ of the TM matrix (measured in units of the bound-state energy of one δ-function potential, $E_{bound} = -\frac{mV_o^2}{2\hbar^2} = -1$). (b) Energy versus Bloch momentum, k, for a static chain. Parameters used are $V_0 = -\sqrt{2}$, $V_1 = 0$, and $l = 5$

It is now interesting to use the Floquet TM matrix derived in Secs.

(3.1) and (3.2) for the case when $V_0 \neq 0, V_1 = 0$ as a way to test the Floquet formalism and to gain insight into the effect of a time periodic perturbation in the band structure of the static potential. Using the Floquet TM matrix of Eq. (3.30) and the same parameters is in Fig.3.3, we obtain in Fig. 3.4a, a plot of the eigenvalues of the TM matrix as a function of the 'quasi-energy'. In Fig.3.4b, we obtain a plot of the 'quasi-energy' vs. Bloch-momentum. The relation between Fig. 3.4 and Fig. 3.3 is simple. The energy axes in Fig.3.3a and 3.3b have been divided into intervals of width $\hbar\omega$ and the intervals have been mapped into the region $0 \leq \epsilon \leq \hbar\omega$ in Figs.3.4a and 3.4b, respectively. The way to recover the results in Fig.3.3 starting with Fig.3.4 is to 'unfold' the quasi-energy axis by calculating the 'average' energy, as defined in Eq. 3.7, for each eigenvector in the Q.E. bands. This shows us that when the oscillating part of the potential is small compared to the static part, the quantity that approximately preserves the band structure of the static potential is $< E >$. The effect of a small oscillating potential is only important when the distance between two unperturbed energy bands is a multiple of $\hbar\omega$ (in the neighborhood of a quasi-energy avoided crossing); this is where the deviations of $< E >$ from the band structure of the static potential occur, as was shown in Figs.3.1 and 3.2. Thus, the average energy is a useful quantity since it smoothly becomes the energy as the oscillating potential is turned off.

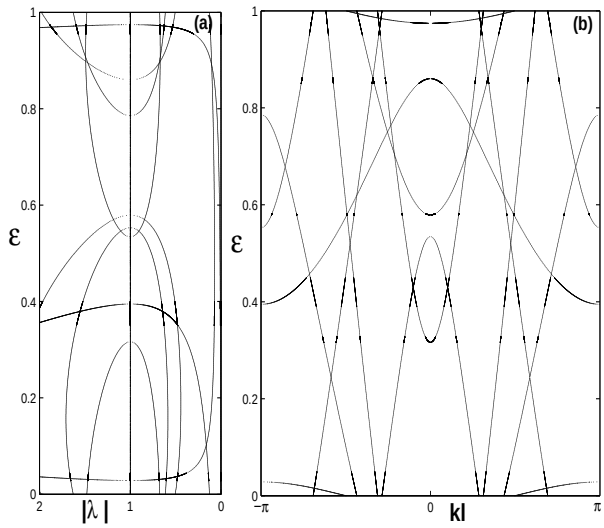

Figure 3.4: (a)Quasienergy, ε, versus the absolute value of the eigenvalues λ of the Floquet TM matrix. (b)Quasienergy, ε, versus the Block momentum, k. Parameters used are $V_0 = -\sqrt{2}$, $V_1 = 0$, and $l = 5$. Only 8 positive energy channels included.

3.4 Eigenvectors of the Floquet Translation Matrix

The solution to the eigenvalue equation (Eq.(3.29)) can be obtained in terms of continued fractions. The procedure we follow is similar to the one used in the study of the scattering properties of a single oscillating δ-function potential [42].

Eq.(3.29) can be written in the form,

$$\begin{aligned} (\mathbf{1} - \mathbf{X})\cdot\mathbf{A} - \mathbf{X}\cdot\mathbf{D} &= \lambda \mathbf{T}_{-l}\cdot\mathbf{A} \\ (\mathbf{1} + \mathbf{X})\cdot\mathbf{D} + \mathbf{X}\cdot\mathbf{A} &= \lambda \mathbf{T}_{l}\cdot\mathbf{D}. \end{aligned} \tag{3.32}$$

Adding these two equations, we obtain a relationship between the components of $\mathbf{A}$ and $\mathbf{D}$,

$$D_n = \eta_n A_n, \quad \text{with} \quad \eta_n = -\frac{1 - e^{ikl}e^{-ik_n l}}{1 - e^{ikl}e^{ik_n l}} \quad , \tag{3.33}$$

where the dimensionless quantities k_n, k and l (defined in Eqs. (3.5) and (3.13)) have been used. The relation between A and D is purely kinematic; it does not depend on the potential. If we combine Eqs. 3.32 and 3.33, we obtain

$$(\mathbf{1} - \lambda \mathbf{T}_{_{-l}}) \cdot \mathbf{A} = \mathbf{X} \cdot \mathbf{P} \cdot \mathbf{A} \tag{3.34}$$

where $\mathbf{P}$ is a diagonal matrix with matrix elements

$$P_n \equiv [\mathbf{P}]_{n,n} = \frac{e^{-ik_n l} - e^{ik_n l}}{1 - e^{ikl} e^{ik_n l}} \; e^{ikl}. \tag{3.35}$$

We now define,

$$Q_n = [\mathbf{1} - \lambda \mathbf{T}_{_{-l}}]_{n,n} = 1 - e^{-ik_n l} e^{ikl}. \tag{3.36}$$

Using this, and Eq.(3.22) we obtain from Eq.(3.34) a three term recursive relation on the components a_n of the eigenvectors of the system,

$$R_n a_n - i h_{n-1} P_{n-1} a_{n-1} = i h_n P_{n+1} a_{n+1}, \tag{3.37}$$

where

$$R_n = Q_n - i s_n P_n. \tag{3.38}$$

Using the method of continued fractions we now obtain from Eq. (3.37) an expression for the ratio $\frac{a_n}{a_{n+1}}$. Let us define

$$f_n = \frac{a_n}{a_{n+1}}. \tag{3.39}$$

If we substitute Eq. (3.39) into Eq.(3.37), we obtain

$$R_n - i h_{n-1} P_{n-1} f_{n-1} = \frac{i h_n P_{n+1}}{f_n}. \tag{3.40}$$

Solving Eq. (3.40) for f_n in terms of f_{n-1} gives,

$$f_n = \frac{ih_n P_{n+1}}{R_n - ih_{n-1}P_{n-1}f_{n-1}}, \tag{3.41}$$

and solving Eq. (3.40) for f_{n-1} in terms of f_n gives

$$f_{n-1} = \frac{1}{ih_{n-1}P_{n-1}}(R_n - \frac{ih_n P_{n+1}}{f_n}). \tag{3.42}$$

Thus, from Eqs. 3.41 and 3.42, we can obtain two different expressions for the quantity f_n. If we iterate Eq. 3.41 we obtain

$$f_n{}^{\downarrow} = \cfrac{ih_n P_{n+1}}{R_n + \cfrac{h_{n-1}^2 P_{n-1}P_n}{R_{n-1} + \cfrac{h_{n-2}^2 P_{n-2}P_{n-1}}{R_{n-2} + \cfrac{h_{n-3}^2 P_{n-3}P_{n-2}}{\vdots}}}} \tag{3.43}$$

where the downward arrow indicates that the indices of all quantities (except P_{n+1}) run over integers equal to or smaller than n. If we iterate Eq. 3.42 we obtain,

$$f_n{}^{\uparrow} = \frac{1}{ih_n P_n}(R_{n+1} + \cfrac{h_{n+1}^2 P_{n+1}P_{n+2}}{R_{n+2} + \cfrac{h_{n+2}^2 P_{n+2}P_{n+3}}{R_{n+3} + \cfrac{h_{n+3}^2 P_{n+3}P_{n+4}}{\vdots}}}), \tag{3.44}$$

where the upward arrow indicates that the indices of all quantities run over integers equal or greater than n. It is important to note that these two functions have very different dependance on n. When $|n| \to \infty$, $f_n{}^{\uparrow} \to \infty$. This implies that for $|n|$ large, $a_n >> a_{n+1}$ (the components of the eigenvector decay for n positive and grow for n negative). On the other hand, when $|n| \to \infty$, $f_n{}^{\downarrow} \to 0$. This implies that for $|n|$ large $a_n << a_{n+1}$ (the components of the

eigenvector grow for n positive and decay for n negative). This means that to obtain eigenvectors that have support in a finite number of channels one has to use ${f_n}^{\uparrow}$ for $n >> 1$ and ${f_n}^{\downarrow}$ for $n << -1$.

We can now derive a general prescription to generate the components of an eigenvector starting from an arbitrary $a_n = 1$. By applying repeatedly the definition of $f_n = \frac{a_n}{a_{n+1}}$, we obtain

$$a_{m+n} = \frac{a_m}{f^{\uparrow}_{m+n-1} f^{\uparrow}_{m+n-2} \cdots f^{\uparrow}_{m}} \tag{3.45a}$$

$$a_{m-n} = f^{\downarrow}_{m-1} f^{\downarrow}_{m-2} \cdots f^{\downarrow}_{m-n} a_m \tag{3.45b}$$

for any $n > 0$. One can avoid having to use both equations to generate the components of an eigenvector by using Eq. 3.45a and starting with an m negative enough so that all eigenvectors have support on channels higher than m. This can be done since for any eigenvector, and for n negative and large, $a_n << a_{n+1}$. Then, the contribution of large negative components to any eigenvector will be negligible.

Let us now define the function,

$$\Pi_n(\varepsilon, k) = \Pi^{n}_{i=-m} \frac{1}{f^{\uparrow}_i(\varepsilon, k)} \tag{3.46}$$

where m is chosen so all eigenvectors have support on channels higher than m. Using this function we can construct the positive momentum components of any eigenvector $\Psi^T = (\mathbf{A^T}, \mathbf{D^T})$, where T denotes transpose, starting with an arbitrarily fixed $a_{-m} = 1$ (before the vector is normalized). We can write

$$\mathbf{A}^T = (..., 1,\ \Pi_{-m}(\varepsilon, k),\ \Pi_{-m+1}(\varepsilon, k),\ ....,\ \Pi_n(\varepsilon, k), ...) \tag{3.47}$$

The negative momentum components, **D**, are obtained from Eq.(3.33).

For any point (ε, k) chosen, there is a band that passes arbitrarily close to that point (the bands fill the first Brillouin zone densely). At this point, several components Π_n have a pole. Each diverging Π_n gives a nonzero component of the eigenvector corresponding to this point. After obtaining the D components and normalizing we end up with the full eigenvector which can be compared to the eigenvectors obtained from direct numerical diagonalization of the matrix TM at the same point.

We have now developed three different methods to obtain Floquet-Bloch states for our system: (1) We can find the eigenvectors of the FB Hamiltonian, Eq. (3.6); (2) We can find the poles of Eq. (3.47); and (3) We can find by numerical diagonalization the eigenvectors of the TM matrix in Eq. (3.30). In the first two approaches, one specifies both the quasi-energy and the Bloch momentum, and then one proceeds to find the corresponding eigenvector. In the third approach, Eq. (3.30), only the quasi-energy is required, the Bloch momentum is a result of the calculation of the eigenvalues of the TM matrix.

In Fig. 3.5a and 3.5b, we show a plot of two eigenfunctions obtained by constructing the translation matrix, TM, for parameters $V_1 = 1.0, V_0 = 0$, and then numerically finding its eigenvalues and eigenvectors. Eigenvector Ψ_1 has quantum numbers, $(\varepsilon = 0.586, k = 0.01)$, and eigenvector Ψ_2 has quantum numbers, $(\varepsilon = 0.07, k = 0.01)$. In Fig. 3.5c we show a graph of the positive momentum components, **A**, and negative momentum components, **D**, of these

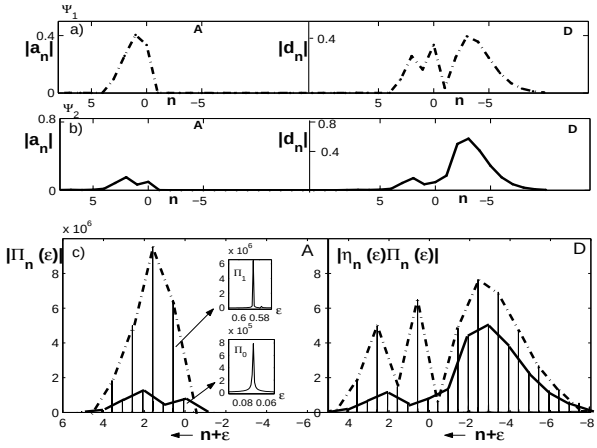

Figure 3.5: Plots of components of **A** and **D** for two FB eigenvectors with $(\varepsilon = 0.586, k = 0.01)$ and $(\varepsilon = 0.07, k = 0.01)$ for $V_0 = 0,\ V_1 = 1.0,\ l = 5$. (a) Eigenvector of the TM matrix with $(\varepsilon = 0.586, k = 0.01)$. (b) Eigenvector of the TM matrix with $(\varepsilon = 0.07, k = 0.01)$. (c) Plots of **A** and **D** obtained from Eqs. (3.47) and (3.33). These plots are indicative of the pole structure of Π_n. The dashed line corresponds to $(\varepsilon = 0.586, k = 0.01)$ and the solid line to $(\varepsilon = 0.07, k = 0.01)$.

eigenvectors as a function of ε for $k = 0.01$, calculated using Eq.(3.47) and Eq.(3.33). The components are arranged in decreasing order of energy (from left to right). There are very narrow peaks for all components shown, at quasi-energies 0.586 and 0.07 as can be seen in the insets. The profile of an eigenstate, as obtained by connecting its corresponding peaks, is in very good agreement with the results obtained by diagonalizing the TM matrix.

By plotting the component $\Pi_8(\varepsilon, k)$ in the interval $0 \leq \varepsilon \leq 1, 0 \leq kl \leq \pi$, one can see the band structure of this potential. We include bands whose eigenvectors have components in channels $n' \leq 8$. Fig. 3.6a shows the Q.E. bands obtained by diagonalizing TM. Fig. 3.6b shows a contour plot of values

of $\Pi_8(\varepsilon, k)$.

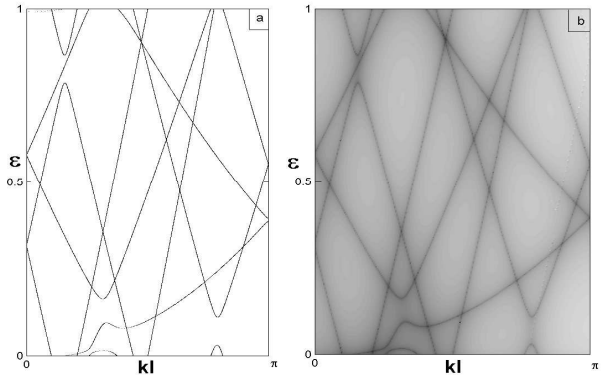

Figure 3.6: $V_0 = 0$, $V_1 = 0.3$, $l = 5$. (a) Quasienergy curves obtained by numerical diagonalization of the Floquet TM matrix. (b) Contour plot of the function $\Pi_8(\varepsilon, kl)$.

As mentioned earlier, feature D in Fig.3.2 can not be explained using degenerate perturbation theory because it is not the result of an avoided crossing. To examine this feature let us consider the functions $f_0^{\downarrow}$ and $f_{-1}^{\downarrow}$, (see Eq. 3.43). When $\varepsilon \to 0$, $h_0 \sim \frac{1}{\sqrt{k_0}} \to \infty$, $h_{-1} \sim \frac{1}{\sqrt{k_0}} \to \infty$ and $P_0 \sim k_0 \to 0$. Therefore $f_0^{\downarrow} \to \infty$ when $\varepsilon \to 0$, which implies $\frac{a_0}{a_1} \to \infty$. One can also show that $f_{-1}^{\downarrow} \to 0$ as $\varepsilon \to 0$, which implies $\frac{a_0}{a_1} \to \infty$. This means that a_0 is the only non-zero component of an eigenvector corresponding to a quasi-energy band at the point $\varepsilon = 0$. Therefore, the average energy of the eigenvector goes to zero at this point. This explains the plunge observed in Fig.3.2 at point D. In principle there should be a feature like D for any band that crosses the line $\varepsilon = 0$. However, the width of the 'plunge' in the average energy band depends on the size of the component a_1 of the eigenvector as one approaches the bottom of the energy Brillouin zone. The higher the average energy of the band where the plunge occurs, the narrower it is, because the a_1 component of the eigenvector is smaller for higher average energies. This result might indicate that a free particle (plane wave) moving with an energy E could be forced to loose all its energy when adiabatically turning on a space-time periodic potential that oscillates with a frequency $\omega = E/\hbar$.

3.5 Contribution of the negative energy channels

In this section we look at an interesting feature of the delta chain, which establishes a nice connection with the scattering properties of a single oscillating δ-function potential. In what follows, we assume the static potential

to be zero ($s_n = 0$ in Eq. 3.38) and ask the question: how do negative energy channels contribute to the Floquet-eigenstates of the system? This question is motivated by the fact that, when the parameter l is large, numerical diagonalization of the TM matrix becomes very inaccurate because the terms $e^{ik_n l}$ become very large for negative energy channels (imaginary momentum k_n). Knowing how those channels contribute to the Q.E. band structure is therefore an important question.

In Fig.3.7a we show the location, in the Q.E. band structure, of two eigenvectors of the system, and in Fig.3.7b we plot the contribution to these eigenvectors from the various Floquet channels. It is important to notice the shape of D in the negative energy channels is very similar for the two eigenvectors despite their different quantum numbers (ε, k). Why is there a peak in channel -5 in all eigenvectors? What determines this structure? For a given amplitude of a_0, the structure of any eigenvector Ψ can be written in the following form,

$$\mathbf{\Psi}^T = (\mathbf{A}^T, \mathbf{D}^T), \tag{3.48}$$

where,

$$\mathbf{A}^T = (..., a_2, a_1, a_0, f^{\downarrow}{}_{-1}a_0, f^{\downarrow}{}_{-2}f^{\downarrow}{}_{-1}a_0, f^{\downarrow}{}_{-3}f^{\downarrow}{}_{-2}f^{\downarrow}{}_{-1}a_0, ...), \tag{3.49}$$

and

$$\mathbf{D}^T = (..., \eta_2 a_2, \eta_1 a_1, \eta_0 a_0, \eta_{-1} f^{\downarrow}{}_{-1}a_0, \eta_{-2} f^{\downarrow}{}_{-2}f^{\downarrow}{}_{-1}a_0, ...). \tag{3.50}$$

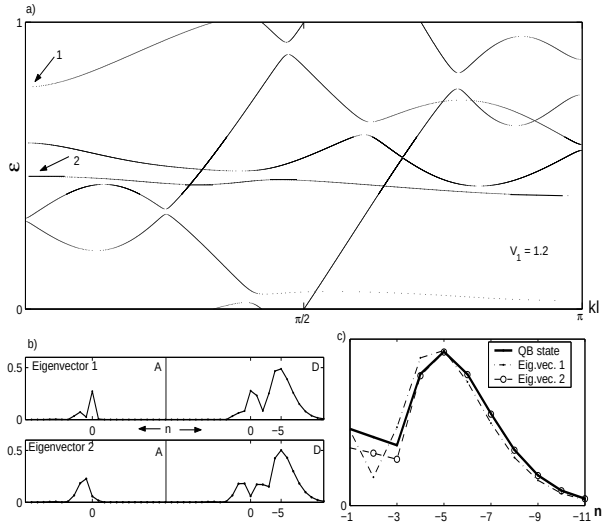

Figure 3.7: (a)Quasienergy band structure for $V_0 = 0,\ V_1 = 1.2,\ l = 5$. Arrows show locations, $(\varepsilon = 0.775, k = 0)$ and $(\varepsilon = 0.462, k = 0)$, of two eigenvectors plotted in Fig. (7b). b) Absolute value of the Floquet components of eigenvectors: (1) $(\varepsilon = 0.775, k = 0)$; and (2) $(\varepsilon = 0.462, k = 0)$. (c) Comparison of the negative energy contributions (D part) of the two eigenvectors in (b) with that of the quasi-bound state of a single δ-function potential.

The structure of the negative energy part of the eigenvectors can be studied by looking at the sequence $(f^{\downarrow}{}_{-1}, (f^{\downarrow}{}_{-2}f^{\downarrow}{}_{-1}), (f^{\downarrow}{}_{-3}f^{\downarrow}{}_{-2}f^{\downarrow}{}_{-1}), ...)$. Let us begin by defining the quantities ρ_n and b_n as

$$\rho_n \equiv \frac{1 - e^{2ik_n l}}{e^{-ikl} - e^{ik_n l}}, \qquad b_n \equiv e^{ik_n l} - e^{ikl}, \tag{3.51}$$

so that

$$P_n = e^{-ik_n l}\rho_n, \qquad R_n = e^{-ik_n l}b_n\ . \tag{3.52}$$

Using this in Eq.(3.43), we obtain an alternative expression for ${f_{-n}}^{\downarrow}$,

$$ {f_{-n}}^{\downarrow} = \cfrac{ih_{_{-n}}\rho_{_{-n+1}}e^{-i(k_{_{-n+1}}-k_{_{-n}})l}}{b_{_{-n}} + \cfrac{h^2_{_{-n-1}}\rho_{_{-n-1}}\rho_{_{-n}}}{b_{_{-n-1}} + \cfrac{h^2_{_{-n-2}}\rho_{_{-n-2}}\rho_{-n-1}}{b_{_{-n-2}} - \cfrac{h^2_{_{-n-3}}\rho_{_{-n-3}}\rho_{_{-n-2}}}{\vdots}}}} \quad . \tag{3.53} $$

For $n > 1$ this expression can be simplified. Since $\rho_{_{-n}} \simeq e^{ikl}$ and $b_n \simeq -e^{ikl}$, $f^{\downarrow}_{-n}$ becomes,

$$ {f_{-n}}^{\downarrow} = \cfrac{ih_{_{-n}}e^{-i(k_{_{-n+1}}-k_{_{-n}})l}}{1 + \cfrac{h^2_{_{-n-1}}}{1 + \cfrac{h^2_{_{-n-2}}}{1 - \cfrac{h^2_{_{-n-3}}}{\vdots}}}} \tag{3.54} $$

From Eq. (3.54), one can conclude that for the negative energy channels, the positive momentum components, **A**, of the eigenvector decay exponentially with n; ${f_{-n}}^{\downarrow} \propto e^{-l/2n}$. This can be seen in Fig. 3.7b where it is evident that the negative energy components of **A** decay very quickly with n. In contrast, the vector, **D**, has a different structure, with a peak at $n = -5$. It is in this part of the eigenvector where the negative energy components contribute the most. If we had chosen to construct the TM matrix for translations to the left, then the A part would have shown the biggest contribution from the negative channels. From Eq. (3.33) and for negative energy channels $d_{-n} \simeq e^{-ik_{_{-n}}l}a_{-n}$. Hence,

$$ \frac{d_{_{-n}}}{d_{_{-n+1}}} = Z_{-n} \equiv \frac{ih_{-n}}{1 + G_{-n}} \quad , \tag{3.55} $$

where the C.F., G_n, can be defined recursively as

$$G_n = \frac{h_{n-1}^2}{1 + G_{n-1}} \quad . \tag{3.56}$$

This function G_n is precisely the same function used to describe the transmission through a single oscillating δ-function[42]. As shown in Appendix A, the ratio between the diagonal components, C_{-n}, of the transmission matrix for a single δ-function is

$$\frac{C_{-n}^*}{C_{-n+1}^*} = -Z_{-n}^{*2} \quad ,$$

where the (*) denotes evaluation at the pole of the S-matrix.

The relationship actually goes further. In appendix B we look at the quasi-bound state of the single δ-function potential and prove that its components (only the transmission part is considered, since the reflection should be identical for symmetry reasons) can be written as,

$$\mathbf{V}_{QB}^T = (....., 1, Z_{-1}^*, Z_{-1}^* Z_{-2}^*, Z_{-1}^* Z_{-2}^* Z_{-3}^*, ...) \tag{3.57}$$

Whereas according to Eq.(3.55), the negative energy components of the vector, $\mathbf{D}$, can be written as

$$\mathbf{D}^T = (....., 1, f_{-1}^{\downarrow}, f_{-1}^{\downarrow} Z_{-2}, f_{-1}^{\downarrow} Z_{-2} Z_{-3}, ...) \quad . \tag{3.58}$$

The difference between Eqs. (3.57) and (3.58) is in the behavior of the function $f_{-1}^{\downarrow}(\varepsilon, k)$, which for a certain range of ε (because of its dependance on the Bloch momentum k) can be considerably different from $Z_{-1}(\varepsilon)$. The other difference concerns the fact that in Eq. (3.57) the Z_{-n} functions are evaluated at the

pole whereas the functions in Eq. (3.58) are evaluated at different values along the bands. In Fig. 3.7b we show two eigenvectors of the infinite chain, and in Fig. 3.7c we compare the negative energy components of $\mathbf{D}$ with the quasi-bound state of the single δ-function system. The agreement is quite good for all the eigenvectors that we considered. The reason for such agreement, which seems to be independent of the particular quasi-energy of the eigenstate, is simple: the functions Z_{-n} are fairly smooth in the complex plane, therefore, their value at E^* and their value on the real axis are very close in most cases.

When the strength, V_1, is small, the different Floquet-eigenstates are exponentially localized about the unperturbed states. As the strength V_1 increases and the eigenstates gain support in the negative energy channels, they develop a characteristic peak in those channels, which can actually dominate the structure of the vector, $\mathbf{D}$, for the eigenstates with lowest average energy.

In general we can say that the structure of all FB eigenvectors of the infinite chain consists of two very distinct parts, the positive energy components which are sensitive to the Bloch-momentum k, and the negative energy components which are independent of k and are closely related to the quasi-bound state of the single δ-function potential. We expect this to be a general feature that should occur in other space-time periodic potentials such as an oscillating Kroenig-Penney potential.

3.6 Band Dynamics

In this section we discuss some general features of the behavior of the quasi-energy bands as the strength V_1 of the oscillating potential is changed. In subsection 3.6.1 we discuss the almost periodic behavior of the Q.E. bands with lowest average energy as V_1 is changed. In subsection 3.6.2 we discuss the existence of points in the Q.E. band structure which are not affected by a change in the parameter V_1. Subsection 3.6.3 deals with the collapse (significant reduction of its width) of one of the Q.E. bands for particular values of V_1.

3.6.1 Periodicity of the band structure

In the sequence of plots in Fig.3.8, we show the bands associated with eigenvectors whose main support is on channels $n \leq 4$. We focus on these bands because they have especially interesting behavior as the parameter V_1 is changed. Inspection of these plots shows that as V_1 is varied, the band patterns come close to repeating their structure in an almost-periodic manner. In going from $V_1 = 0$ to $V_1 = 1.0$ there is one complete exchange of identity for each band: (0,0) $\rightarrow$ (0,-1)-(1,1), (0,-1)-(1,1)$\rightarrow$ (1,-1)-(2,1), (1,-1)-(2,1)$\rightarrow$ (0,0). From $V_1 = 1.0$ to $V_1 = 1.414$ there is another exchange. This periodicity occurs as a function of V_1^2. A similar quasi-periodic behavior was found for the transmission through a single oscillating delta function potential [42], where the dynamics of the zeros and poles of the system depend almost periodically on the parameter $a \equiv V_1^2$. The period in V_1^2 is one: the equivalent of panel

$V_1^2 = 0.25$ is panel $V_1^2 = 1.25$, the equivalent of panel $V_1^2 = 0.5$ is $V_1^2 = 1.5$, and so on. This periodicity is another manifestation of the correlation between the structure of the quasi-bound state in the single delta scattering problem and the structure of the eigenvectors with support in the lowest energy channels in the infinite chain.

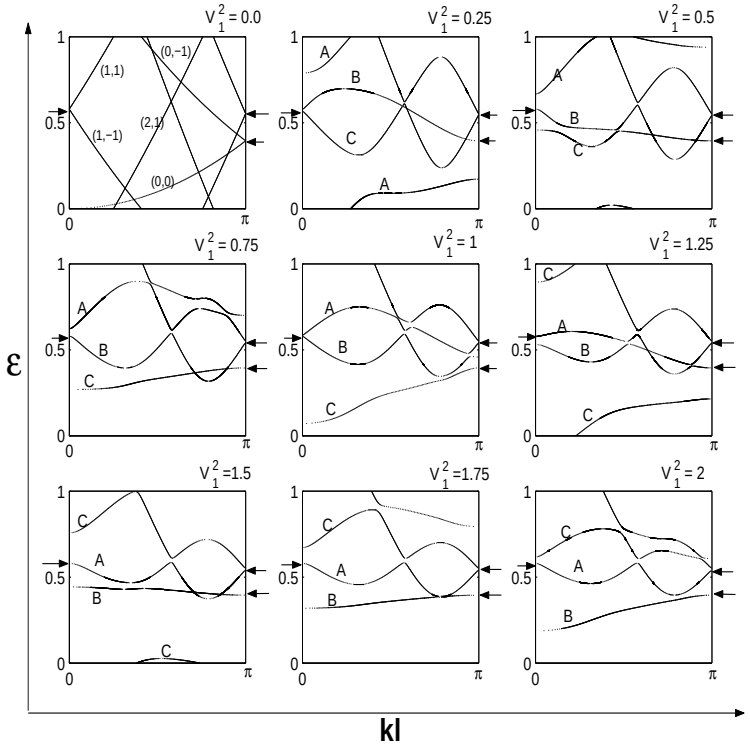

Figure 3.8: Series of plots showing the evolution of Q.E bands (the four lowest in average energy) as the parameter V_1 is increased with fixed $V_0 = 0$ and $l = 5$. Three of the bands (A,B,C) participate in a periodic exchange of identity. Band A initially related to unperturbed state (0,0), band B related to unperturbed states (1,1),(0,-1) and band C related to states (1,-1), (2,1). Arrows indicate the position of some of the fixed points in the Q.E. band structure.

3.6.2 Fixed points in the band structure

Suppose that before we turn on the oscillating potential, we have a state which is a superposition of two plain waves, in particular $\phi_n(x) = \frac{1}{2i}(e^{ik_n x} - e^{-ik_n x}) = \sin(\mathrm{k_n x})$. If k_n satisfies the condition, $k_n = m\pi/l$ with $-\infty \leq m \leq \infty$, then $\sin(\mathrm{k_n l}) = 0$, which means that the wave function has nodes at the location of the δ-functions. This implies that this particular state will not be affected as the potential is turned on (whether the δ-function potential is oscillating or not). This state is a Bloch state since it is periodic in space and it must belong to a band of the perturbed system. Therefore, for an infinite chain of δ-functions, oscillating or not, there are fixed points in the band structure, in the sense that for any V_1 and V_0 there is always a band attached to the points that satisfy the condition $k_n = m\pi/l$. This is a special feature of the delta function potential. The fixed points are at the edges (m odd) and the center (m even) of the Brillouin zone. For $l = 5$, we can obtain the location in quasi-energy of the fixed points,

$$\sqrt{\varepsilon_{m,n} + n} = m\pi/l \tag{3.59}$$

From this and the additional condition $0 \leq \varepsilon_{m,n} \leq 1$ we obtain the first three, $\varepsilon_{0,1} = 0.395$, $\varepsilon_{1,2} = 0.579$, and $\varepsilon_{3,3} = 0.553$. The value $\varepsilon_{0,0} = 0$ is not important because the wave function of this state vanishes everywhere.

These three fixed points have been marked with arrows in the different panels in Fig.3.8. It is important to mention that there are an infinite number of these points. In the panels in Fig.3.8, only those associated with the positive

energy channels, $n \leq 4$ are shown. The higher energy channels are not coupled in a significant way with the bands shown and do not produce any significant change in them.

3.6.3 Band Collapse

As can be seen in Fig.3.9a, near the value $V_1 = 0.767$, one of the three Q.E. bands that participated in the exchange described in Section 3.6.1 becomes practically flat, that is, the width of that Q.E. band has collapsed to its minimum value. This collapse occurs almost periodically as a function of V_1^2. Collapse of Q.E. bands in a periodic potential driven by a oscillating electric field has been studied before using one-band and two-band approximations [30]. It was shown there that in the single-band nearest neighbor tight binding approximation, the collapse is complete (the width of the band goes to zero) and is determined by the zeros of the Bessel function J_0. In the same paper, numerical calculations show that the collapse is not complete as it is expected from the von Neumann-Wigner non-crossing rule [43].

The probability current associated with an eigenstate in a collapsed band is very small. For $l = 5$, only the positive energy components of an eigenstate could contribute to this current since the current due to the negative energy components is already very small (it decays exponentially with l). Because of this, each oscillating δ-function in the chain must reflect the incident positive energy components of an eigenstate in a collapsed band. This is only possible if the location in quasi-energy of the collapsed band is close to the

quasi-energy value for which a transmission zero occurs in a single δ-function potential [42].

In Fig.3.9a, the transmission probability through one δ-function has been plotted alongside the band structure of the infinite chain shown in Fig.3.9b. This figures shows that the location of the collapsed band and the location of the zero of transmission are very close. Other collapses are expected for values of V_1 that satisfy the approximate relation $V_1^2\ (mod 1) \approx 0.767$. A relationship between the suppression of tunnelling and band collapse has been pointed out before by Gomez-Llorente et al.[44], although within the two-band approximation.

In Fig.3.9c, we enlarge the region occupied by the collapsed band. It reveals that the band has a finite width $\Delta \approx 0.008\hbar\omega$. Several avoided crossings with other bands can be seen. In Fig. (3.9d) we only needed to include Floquet channels with $n \leq 1$ in the calculation , which shows that the basic structure of the band is determined by the coupling between the first propagating channel (n=0) and the negative energy channels. Another way to obtain this basic structure is by using the diabatic representation, [45],[46] where all avoided crossings with a gap smaller than a certain value are replaced by crossings. In Fig.(3.9d), superimposed on the band is a plot of the function cos(2kl), which corresponds to the shape of the band if only nearest-neighbor interaction is allowed. The relative displacement of the maxima in the two curves indicates that there is a small amount of direct coupling between non-adjacent cells. In Fig. 3.9e we show the average energy of the eigenstate associated with the col-

lapsed band and also the structure of two eigenstates at the points indicated. Near the edges of the Brillouin zone (the fixed point) the structure of the eigenstate is dominated by the structure of the unperturbed state, $\sin(k_0 x)$, which carries no current. The energy of the Floquet eigenstate near these points is therefore positive. As one moves from the edge to the center of the Brillouin zone the negative energy channels dominate and the average energy becomes negative.

It has been shown before that a relationship exists between dynamical suppression of tunnelling and band collapse. In this work we have shown a relationship between dynamical suppression of transmission and band collapse. Other localized potentials such as the square well (or barrier) have been shown to have transmission zeros (resonances)[23, 24] and therefore one might expect to observe Q.E. band collapses associated with periodic chains of these potentials.

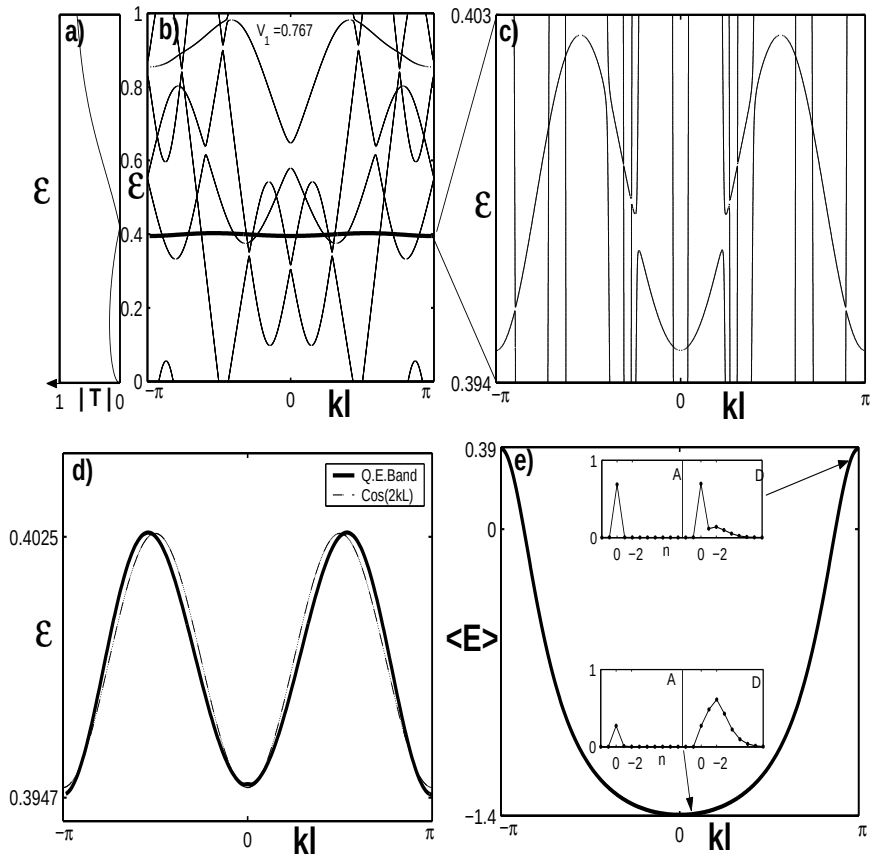

Figure 3.9: (a)The transmission probability for a single oscillating δ-function potential as a function of quasienergy for $V_0 = 0,\ V_1 = 0.767,\ l = 5$. (b) The quasienergy band structure of the infinite chain for $V_0 = 0,\ V_1 = 0.767,\ l = 5$. The collapsed Q.E. band is the thick line. (c) Magnification of the region in (b) occupied by the collapsed band. (d) The band (solid line) without the small avoided crossings with higher energy bands (diabatic representation). The function cos(2kl) is plotted for comparison (dot-dashed line). (e) The average energy along the collapsed band and the components of eigenstates from two different locations on the collapsed band.

Chapter 4

Floquet-Green's function formalism for harmonically driven Hamiltonians

4.1 Introduction

In chapter 2 we studied a simple model of a localized time-harmonic potential; in chapter 3 we developed a method to derive the quasi-energy band structure of a space-time harmonic system composed of an infinite chain of the previously studied oscillating delta-functions. For this chapter we develop a generalization of the method used in the previous two chapters to solve a three term recursion relation. With this generalization we are able write a general expression for the solution of any harmonically driven(HD) potential.

As we have mentioned before, in the last two decades, HD potentials (space periodic or not), have been studied considerably and many interesting effects have been found. Among them: dynamical localization (mini-band collapse)[30, 31], photon-assisted tunnelling [32], quantum hamiltonian ratchets [33, 34], chaos-assisted tunnelling [35–39, 49] and atom stabilization [50]. They have also been used to study quantum tunnelling time [16–18], ionization [19, 51], electronic transmission [21–24, 42], and quantum chaos [15].

The pioneering work of Shirley[52] and Sambe[6] laid down the theoret-

ical foundations for a complete treatment of time-periodic potentials, based on the same mathematical tools already developed for time-independent potentials. Of great importance among these tools is the Green's function, whose definition and application for time-periodic systems has not been clear until recently. A Floquet-Green's function method for the solution of radiative electron scattering in a strong laser field was introduced by F.H.M Faisal[53]. More recently, the t-t' method [7] for treating time-dependent systems was developed with great success. For the case of a periodic potential this formalism provides a natural way of defining and using the Floquet-Green's function which can be used to study scattering through this kind of potential [7]. For the case of a Harmonic Driving (HD) potential we find the Floquet Hamiltonian and derive the Floquet-Green's function of the system using Matrix Continued Fractions (MCF). This same approach can be used to derive the Green's function of a phonon-coupled system, given the close resemblance between these two systems[54, 55]. It has in fact been used for the case of a two state system coupled to a harmonic oscillator.[56]

As an application of our method we calculate the Floquet-Green's function for a system whose Hamiltonian is periodic in space (we use the tight binding approximation) and has a defect at a particular location in the lattice. We characterize the defect by its on-site energy, which changes harmonically in time as $V_0 + V_1 cos(\omega t)$. This hamiltonian could be realized experimentally in a 1-D hetero-structure where a metal contact has been placed covering a small region and is connected to an oscillating voltage source. We also believe

that the problem of conduction through a molecule placed between two metal contacts could be modelled with a similar Hamiltonian.

In section 4.2 we introduce the Floquet Hamiltonian and the Floquet-Green's function for a time-periodic system. In section 4.3 we derive the Floquet-Green's function for the case of a HD potential using matrix continued fractions. In section 4.4, as an illustration of the technique developed in section 4.3, we study a tight-binding Hamiltonian with a defect energy which depends harmonically on time. We calculate the Local Density of States (LDOS) and study the existence of localized states and their behavior as a function of the different parameters of the model.

4.2 t-t' method and Floquet-Green's function

In our approach we use the (t,t') method [7] where the time variable t' is treated as a spatial coordinate, and a new quasi-time variable t is introduced. Using this approach we derive the expression for the Floquet-Green's function of a general time-periodic system.

We introduce the Floquet-Hamiltonian, H^F, which is defined as

$$H^F(x,t') = H(x,t') - i\hbar\frac{\partial}{\partial t'} \quad , \tag{4.1}$$

and the (t,t')-Schrödinger equation

$$i\hbar\frac{\partial}{\partial t}\chi(x,t,t') = H^F(x,t')\chi(x,t',t) \quad . \tag{4.2}$$

It is easy to show, that if $\chi(x,t',t)$ satisfies Eq.(4.2), then

$$\phi(x,t) \equiv \chi(x,t,t) \tag{4.3}$$

is a solution to the Schrödinger equation

$$i\hbar\frac{\partial}{\partial t}\phi(x,t) = H(x,t)\phi(x,t) \quad . \tag{4.4}$$

The great advantage of the t-t' method is that, since the Hamiltonian (Eq.4.2) is independent of t, $\chi(x,t',t)$ can be found using the standard techniques developed for time independent Hamiltonian.

By using the method of separation of variables, we can write

$$\chi(x,t,t') = e^{-i\epsilon t/\hbar}\psi(\epsilon|x,t'), \tag{4.5}$$

and using this into Eq.(4.2), gives a t-independent Schrödinger equation

$$H^F(x,t')\psi(\epsilon|x,t') = \epsilon\psi(\epsilon|x,t') \quad . \tag{4.6}$$

As a consequence of Floquet's theorem, if $H(x,t')$ is periodic in t'(period τ), $\psi(\epsilon|x,t')$ is also periodic in t'. We define the Green's function corresponding to this Floquet-Hamiltonian as:

$$[\epsilon - H^F(x,t')]G^F(\epsilon|x,x',t',t") = \delta(x-x')\delta_\tau(t'-t") \quad , \tag{4.7}$$

where $\delta_\tau(x)$ is the τ-periodic delta function. Because of the periodicity of the Hamiltonian, the Floquet eigenfunctions as defined by Eq.(4.6) are periodic in time. The solution of Eq.(4.7) can be written as

$$G^F(\epsilon|x,x',t',t") = \int d\epsilon' \sum_n \frac{\psi_n^*(\epsilon'|x,t')\psi_n(\epsilon'|x',t")}{\epsilon-\epsilon'} \quad , \tag{4.8}$$

where $\{\psi_n(\epsilon'|x,t)\}$ is the complete set of eigenfunctions of the Floquet-Hamiltonian (Eq.4.6). From this expression it can be seen that $G^F(\epsilon|x,x',t',t")$ is periodic in both t' and t", therefore, it can be written as

$$G^F(\epsilon|x,x',t',t") = \sum_{\alpha,\beta=-\infty}^{\infty} G^F_{\alpha,\beta}(\epsilon|x,x')e^{i\alpha t'}e^{-i\beta t"} \quad . \tag{4.9}$$

Similarly for $H^F(x,t')$ we write

$$H^F(x,t') = \sum_{\gamma=-\infty}^{\infty} H^F_\gamma(x)e^{i\gamma t'} \quad . \tag{4.10}$$

Using Eqs.(4.9),(4.10) into (4.7) and equating components we get

$$\epsilon\, G^F_{\alpha,\beta}(\epsilon|x,x') - \sum_{\gamma=-\infty}^{\infty} H^F_{\alpha,\gamma}(x)G^F_{\gamma,\beta}(\epsilon|x,x') = \delta(x-x')\delta_{\alpha,\beta} \quad , \tag{4.11}$$

where $H^F_{\alpha,\gamma} \equiv H^F_{\alpha-\gamma}$.

In the next section we specialize Eq.(4.11) for the case of a HD Hamiltonian. We will use the method of matrix continued-fractions (MCF) to derive an explicit solution for the Floquet-Green's function assuming a potential that depends harmonically on time.

4.3 Harmonically Driven Potential, Matrix CF method

The Hamiltonian that we consider in this part is of the general form (with no particular representation chosen),

$$\mathcal{H} = \mathcal{H}^o + \mathcal{V}_o + 2\mathcal{V}_1 cos(\omega t'). \tag{4.12}$$

This general class of Hamiltonians includes a great variety of physical systems of interest. We refer to this class of Hamiltonians as harmonically driven (HD) Hamiltonians. In section 4.4 we will apply the methods developed here to a simple but nonetheless interesting system: A tight-binding model with a defect on-site energy that depends harmonically on time. According to Eqs.(4.1),(4.10) and the definition after Eq.(4.11), the Floquet-Hamiltonian corresponding to Eq.(4.12) is

$$\mathcal{H}^F_{\alpha,\gamma} = (\mathcal{H}^o + \mathcal{V}_o - \alpha\hbar\omega)\delta_{\alpha,\gamma} + \mathcal{V}_1(\delta_{\alpha+1,\gamma} + \delta_{\alpha-1,\gamma}) \quad . \tag{4.13}$$

Using this into Eq.(4.11) we get

$$(\mathtt{1}E_\alpha - \mathcal{H}^S)\mathcal{G}_{\alpha,\beta} - \mathcal{V}_1(\mathcal{G}_{\alpha+1,\beta} + \mathcal{G}_{\alpha-1,\beta}) = \mathtt{1}\delta_{\alpha,\beta} \quad , \tag{4.14}$$

where

$$E_\alpha \equiv \varepsilon + \alpha\hbar\omega, \qquad \mathcal{H}^S \equiv \mathcal{H}^o + \mathcal{V}_o \ , \qquad < x|\mathcal{G}_{\alpha,\beta}|x' > \equiv G^F_{\alpha,\beta}(\epsilon|x,x') \quad . \tag{4.15}$$

To solve Eq.4.14 we use MCF. It basically follows the procedure introduced by Martinez et al,[42, 57] which has also been used by Moskalets and Büttiker [58] for the solution of a three-term recurrence relations in a HD system. Similar approaches using CF's have also been used before in the solution

of time-independent Hamiltonians (tight binding type).[9, 10, 59] To begin, we define the operator

$$\mathcal{F}_{\alpha,\beta} \equiv \mathcal{G}_{\alpha,\beta}\mathcal{G}^{-1}_{\alpha+1,\beta}, \tag{4.16}$$

from which we can write

$$\mathcal{F}^{-1}_{\alpha,\beta}\mathcal{G}_{\alpha,\beta} = \mathcal{G}_{\alpha+1,\beta} \quad ,$$

$$\mathcal{F}_{\alpha-1,\beta}\mathcal{G}_{\alpha,\beta} = \mathcal{G}_{\alpha-1,\beta} \quad . \tag{4.17}$$

Using this equations into Eq.(4.14) we get,

$$(\mathtt{1}E_\alpha - \mathcal{H}^S)\mathcal{G}_{\alpha,\beta} - (\mathcal{V}_1\mathcal{F}^{-1}_{\alpha,\beta} + \mathcal{V}_1\mathcal{F}_{\alpha-1,\beta})\mathcal{G}_{\alpha,\beta} = \mathtt{1}\delta_{\alpha,\beta} \quad . \tag{4.18}$$

Let us consider this equation for the case $\alpha \neq \beta$,

$$(\mathtt{1}E_\alpha - \mathcal{H}^S)\mathcal{G}_{\alpha,\beta} - (\mathcal{V}_1\mathcal{F}^{-1}_{\alpha,\beta} + \mathcal{V}_1\mathcal{F}_{\alpha-1,\beta})\mathcal{G}_{\alpha,\beta} = 0 \qquad \text{for} \qquad \alpha \neq \beta \ . \tag{4.19}$$

A trivial solution of this equation is $\mathcal{G}_{\alpha,\beta} = 0$, for $\alpha \neq \beta$; that is, the off-diagonal components vanish. This is expected only for the case $V_1 = 0$. For $V_1 \neq 0$ we assume that in general the off diagonal elements do not vanish (at least not all of them) and therefore, from Eq.(4.19) we get,

$$\mathtt{1}E_\alpha - \mathcal{H}^S = (\mathcal{V}_1\mathcal{F}^{-1}_{\alpha,\beta} + \mathcal{V}_1\mathcal{F}_{\alpha-1,\beta}) \qquad \text{for} \qquad \alpha \neq \beta \ . \tag{4.20}$$

Evaluating this equation for $\alpha = \beta + 1$, we get

$$\mathcal{V}_1\mathcal{F}_{\beta,\beta} = \mathcal{C}_{\beta+1} - \mathcal{V}_1(\mathcal{V}_1\mathcal{F}_{\beta+1,\beta})^{-1}\mathcal{V}_1, \tag{4.21}$$

where, to simplify notation we defined $\mathcal{C}_\beta \equiv \mathtt{1}E_\beta - \mathcal{H}^S$. Iterating Eq.(4.21) we get,

$$\mathcal{V}_1\mathcal{F}_{\beta,\beta} = \mathcal{C}_{\beta+1} - \mathcal{V}_1 \cfrac{1}{\mathcal{C}_{\beta+2} - \mathcal{V}_1 \cfrac{1}{\mathcal{C}_{\beta+3} - \mathcal{V}_1 \cfrac{1}{\vdots}\mathcal{V}_1}\mathcal{V}_1}\mathcal{V}_1 \quad . \tag{4.22}$$

Here, the notation $\frac{1}{A}$ instead of A^{-1} has been used for clarity. Evaluating Eq.(4.19) for $\alpha = \beta - 1$ we get

$$\begin{aligned} \mathcal{V}_1\mathcal{F}^{-1}_{\beta-1,\beta} &= \mathcal{C}_{\beta-1} - \mathcal{V}_1(\mathcal{F}_{\beta-2,\beta}\mathcal{V}_1^{-1})\mathcal{V}_1, \\ &= \mathcal{C}_{\beta-1} - \mathcal{V}_1 \frac{1}{\mathcal{V}_1\mathcal{F}^{-1}_{\beta-2,\beta}}\mathcal{V}_1 \quad . \end{aligned} \tag{4.23}$$

Continuing the fraction in an iterative way we get,

$$\mathcal{V}_1\mathcal{F}^{-1}_{\beta-1,\beta} = \mathcal{C}_{\beta-1} - \mathcal{V}_1 \cfrac{1}{\mathcal{C}_{\beta-2} - \mathcal{V}_1 \cfrac{1}{\mathcal{C}_{\beta-3} - \mathcal{V}_1 \cfrac{1}{\vdots}\mathcal{V}_1}\mathcal{V}_1}\mathcal{V}_1. \tag{4.24}$$

We now rewrite Eq.(4.18), for $\alpha = \beta$ as

$$(\mathtt{1}E_\beta - \mathcal{H}^S)\mathcal{G}_{\beta,\beta} - (\mathcal{V}_1(\mathcal{V}_1\mathcal{F}_{\beta,\beta})^{-1}\mathcal{V}_1 + \mathcal{V}_1(\mathcal{V}_1\mathcal{F}^{-1}_{\beta-1,\beta})^{-1}\mathcal{V}_1)\mathcal{G}_{\beta,\beta} = \mathtt{1} \ . \tag{4.25}$$

Using Eqs.(4.22) and (4.24) we finally get

$$(\mathtt{1}E_\beta - \mathcal{H}^S - \mathcal{V}_{eff}(E_\beta))\mathcal{G}_{\beta,\beta}(\varepsilon) = \mathtt{1} \ , \tag{4.26}$$

where

$$\mathcal{V}_{eff}(E_\beta) = \mathcal{V}^{\uparrow}_{eff}(E_\beta) + \mathcal{V}^{\downarrow}_{eff}(E_\beta) \quad , \tag{4.27}$$

with

$$\mathcal{V}^{\uparrow}_{eff}(E_\beta) = \mathcal{V}_1 \cfrac{1}{\mathcal{C}_{\beta+1} - \mathcal{V}_1 \cfrac{1}{\mathcal{C}_{\beta+2} - \mathcal{V}_1 \cfrac{1}{\vdots}\mathcal{V}_1}\mathcal{V}_1}\mathcal{V}_1 \quad ,$$

$$\mathcal{V}^{\downarrow}_{eff}(E_\beta) = \mathcal{V}_1 \cfrac{1}{\mathcal{C}_{\beta-1} - \mathcal{V}_1 \cfrac{1}{\mathcal{C}_{\beta-2} - \mathcal{V}_1 \cfrac{1}{\vdots}\mathcal{V}_1}\mathcal{V}_1}\mathcal{V}_1 \quad . \tag{4.28}$$

The off-diagonal components of the Floquet-Green's function operator can be calculated by repeated multiplication by the operators $\mathcal{V}^{\uparrow}_{eff}$ and $\mathcal{V}^{\downarrow}_{eff}$.

Eq.(4.26) is very interesting. It gives an expression for the diagonal part of the Floquet-Green's function of the system (from which elastic transmission and density of states can be calculated), in which the effect of the coupling between different (Floquet) channels, generated by the HD potential, has been "summed up" into a dynamical effective potential (D.E.P.) that is energy dependent. This general result for the class of HD Hamiltonians is related to the "pruning" technique developed by Bonča and Trugman [60] for the treatment of electron-phonon interactions within a tight-binding lattice. Also, Pastawski et al.[59] have developed a similar method ("decimation" technique) for the treatment of electron transport through a molecule.

It is interesting to notice from Eq.(4.28) that to lowest order in E and $\mathcal{V}_1$, we get $\mathcal{V}_{eff} = -\mathcal{V}_1(\mathcal{H}^S)^{-1}\mathcal{V}_1$, which means that the harmonic potential generates an energy independent D.E.P. which is negative (in general it will lower the energy of the perturbed eigenstates as compared to the energy of the unperturbed ones) and is quadratic in V_1. The effect of this quadratic

dependence of the effective potential has been reported before regarding the dependence of the transmission zero and pole with the amplitude of the oscillating potential for a δ-function potential[42] and also regarding the dynamics of the quasi-energy bands with lowest average energy in a chain of oscillating δ-function potentials [57]. This lowest-order correction to the potential experienced by a particle in an oscillating potential is similar to the so called Franck-Condon energy which is also negative and quadratic in the coupling constant between electrons in a lattice and phonons. [61]

It is also worth noticing that our formalism goes beyond any perturbative approach in $\mathcal{V}_1$ since, even if we truncate the expression for $\mathcal{V}_{eff}$ to lowest order in $\mathcal{V}_1$, which gives, $\mathcal{V}_{eff}(E_\beta) \sim \mathcal{V}_1(\frac{1}{\mathcal{C}_{\beta+1}} + \frac{1}{\mathcal{C}_{\beta-1}})\mathcal{V}_1$, the resulting expression for $\mathcal{G}_{\beta,\beta}$ contains all even powers of V_1. This means that truncation of $\mathcal{V}_{eff}$ to lowest order still gives a Floquet-Green's function which includes contributions of an infinite number of diagrams. This feature makes Eq.(4.26) an ideal framework for the treatment of very strong HD potentials such as the ones produced by laser fields where multiphoton processes are common[62], and interesting effects such has atom stabilization have been reported.[50]

Finally, we notice that the dependence of any quantity in Eq.(4.26) on the index β is only through the "channel" energy $E_\beta = \varepsilon + \beta\hbar\omega$, where the quasienergy ε (usually taken to be $\varepsilon \in [0, 1]\hbar\omega$) appears adding to $\beta\hbar\omega$. Because of this, the index β in E_β will be dropped. E represents the main channel energy, which, for example, in a scattering problem through this kind of potential, corresponds to the energy of the incoming particle. We can

therefore simplify even further the notation in Eq.(4.26):

$$\mathcal{G}^D(E) = \frac{1}{(\mathtt{1}E - \mathcal{H}^S - \mathcal{V}_{eff}(E))} \quad , \tag{4.29}$$

where $\mathcal{G}^D(E) = \mathcal{G}^D(\varepsilon + \alpha\hbar\omega) \equiv \mathcal{G}_{\alpha,\alpha}(\varepsilon)$.

Eq.(4.29) can also be written making use of the Green's function corresponding to the time independent part of the Hamiltonian,

$$\mathcal{G}^D = \mathcal{G}^S \frac{1}{\mathtt{1} - \mathcal{V}_{eff}(E)\mathcal{G}^S} \quad , \tag{4.30}$$

with

$$\mathcal{G}^S \equiv \frac{1}{\mathtt{1}E - \mathcal{H}^S} \quad . \tag{4.31}$$

4.4 Tight-binding with defect. HD site-energy case

Electron localization in a crystal due to defects has been studied for many decades. In a space-periodic (time independent) potential described in the tight-binding approximation, an irregularity in the atomic potential generates a bound state localized in the neighborhood of the defect[63]. If the energy mismatch between the site-energy of the defect and that of the medium in which it is embedded is V_0, the energy of the localized state is found to be $sign(V_0)\sqrt{4T^2 + V_0^2}$, where T is the tunnelling parameter and the allowed band of extended states corresponds to energies between $-2T$ and $2T$.

The system we are interested in, also couples the electron at the impurity with a HD field. This system is similar to a tight-binding hamiltonian

with a defect that couples the electron states with the degrees of freedom of localized phonons.[14] As it has been shown before[54], the transmission in these two systems can be derived from a similar set of equations and therefore presents several features in common. The main differences are: 1) The harmonic oscillator spectrum of the phonons is bounded from below, which implies that it is impossible for an electron to gain energy when interacting with a harmonic oscillator in the ground state. For a HD potential, the electron can always gain energy (or loose it). 2) The coupling between a state with the harmonic oscillator in the eigenstate N, and a state with a harmonic oscillator in state N+1 or N-1, depends on N: for initial electron energy E and initial phonon state N, the probability amplitude to be scattered into the electron state E-$\hbar\omega$ and phonon state N+1 is proportional to $\sqrt{N+1}$; for E+$\hbar\omega$ and phonon state $N-1$ it is $\sqrt{N}$. This is not the case for the time periodic field for which this probability amplitudes do not depend on any parameter except the amplitude of the HD field. 3) Phonons are usually due to thermal vibrations, which means that temperature is an additional variable to be considered in electron-phonon coupled systems. It is not a consideration for a HD potential which can be realized only by the application of an external field onto the electron system. Despite these differences, the two systems can be solved in an almost identical way, and the differences can only be attributed to the thermal averaging (necessary in the phonon case) when the oscillator state, before the interaction with the electron, has a large N.

We will apply the method developed in the last section, now for the

case of a Hamiltonian which has its matrix elements in the site representation given by

$$\mathcal{H} = \mathcal{H}^0 + (V_0 + V_1 cos(\omega t))|0 >< 0|, \tag{4.32}$$

with

$$\mathcal{H}^0 \equiv -T \sum_j (|j+1 >< j| + |j-1 >< j|), \tag{4.33}$$

where t is associated with the tunnelling probability between adjacent sites in the lattice, V_0 characterizes the defect on-site energy and V_1 is the amplitude of the external HD field, which is assumed to exist only at the defect site ($j = 0$ site). We have taken the on-site energy throughout the lattice to be zero except at the defect location.

In the notation of Eqs. (4.12),(4.15) we have

$$\begin{aligned} \mathcal{H}^D &= \mathcal{H}^0 + \ V_0|0 >< 0|, \\ \mathcal{V}_1 &= \frac{1}{2} V_1 |0 >< 0| \ \ . \end{aligned} \tag{4.34}$$

From this, and using Eq.(4.27) and (4.28) we get

$$\begin{aligned} \mathcal{V}^{\uparrow}_{eff}(E) &= \frac{1}{4} V_1^2 |0 >< 0| \frac{1}{\mathcal{C}_1(E) - |0 >< 0| \mathcal{V}^{\uparrow}_{eff}(E+1)|0 >< 0|} |0 >< 0| \\ &= V^{\uparrow}_{eff}(E)|0 >< 0| \ \ , \end{aligned} \tag{4.35}$$

where the function $V^{\uparrow}_{eff}(E)$ is defined as

$$V^{\uparrow}_{eff}(E) \equiv \frac{1}{4}V_1^2 < 0|\frac{1}{\mathcal{C}_1(E) - V^{\uparrow}_{eff}(E+1)\ |0><0|}|0> \quad . \tag{4.36}$$

Similarly for $\mathcal{V}^{\downarrow}_{eff}(E)$ we get

$$\begin{aligned}\mathcal{V}^{\downarrow}_{eff}(E) &= \frac{1}{4}V_1^2|0><0|\frac{1}{\mathcal{C}_{-1}(E) - |0><0|\mathcal{V}^{\uparrow}_{eff}(E-1)|0><0|}|0><0| \\ &= V^{\downarrow}_{eff}(E)|0><0| \quad ,\end{aligned} \tag{4.37}$$

where the function $V^{\downarrow}_{eff}(E)$ is defined as

$$V^{\downarrow}_{eff}(E) \equiv \frac{1}{4}V_1^2 < 0|\frac{1}{\mathcal{C}_{-1}(E) - V^{\downarrow}_{eff}(E-1)\ |0><0|}|0> \quad . \tag{4.38}$$

Accordingly, the operator $\mathcal{V}_{eff}(E)$ can be written as

$$\mathcal{V}_{eff}(E) = V_{eff}(E)|0><0| = (V^{\downarrow}_{eff}(E) + V^{\uparrow}_{eff}(E))|0><0| \quad . \tag{4.39}$$

Using this into Eq.(4.29) we get

$$\mathcal{G}^D(E) = \frac{1}{(\mathtt{1}E - \mathcal{H}^0 - (V_0 + V_{eff}(E))|0><0|)} \quad . \tag{4.40}$$

In terms of the Green's function for the operator $\mathcal{H}^0$ we write

$$\mathcal{G}^D(E) = \mathcal{G}^0\frac{1}{(\mathtt{1} - H_1(E)\mathcal{G}^0)} \quad , \tag{4.41}$$

where

$$\mathcal{G}^0 = \frac{1}{(\mathtt{1}E - H^0)} \quad , \quad \text{and} \quad H_1(E) = (V_0 + V_{eff}(E))|0><0| = V(E)|0><0|. \tag{4.42}$$

The operator $(\mathtt{1} - H_1(E)\mathcal{G}^0)^{-1}$ can be evaluated easily,

$$\begin{aligned}\frac{1}{(\mathtt{1} - H_1(E)\mathcal{G}^0)} &= \mathtt{1} + V(E)|0><0|\mathcal{G}^0 + V(E)^2\mathcal{G}^0_{0,0}|0><0|\mathcal{G}^0 + ... \\ &= \mathtt{1} + \frac{V(E)}{1 - V(E)\mathcal{G}^0_{0,0}}|0><0|\mathcal{G}^0 \quad ,\end{aligned} \tag{4.43}$$

and therefore,

$$\mathcal{G}^D = \mathcal{G}^0 + \frac{V(E)}{1 - V(E)\mathcal{G}^0_{0,0}}\mathcal{G}^0|0><0|\mathcal{G}^0 \quad . \tag{4.44}$$

In the site representation this equation reads

$$\mathcal{G}^D_{i,j} = \mathcal{G}^0_{i,j} + \frac{V(E)}{1 - V(E)\mathcal{G}^0_{0,0}}\mathcal{G}^0_{i,0}\mathcal{G}^0_{0,j} \quad , \tag{4.45}$$

and for $i = j = 0$, we get

$$\begin{aligned}\mathcal{G}^D_{0,0} &= \mathcal{G}^0_{0,0} + \frac{V(E)}{1 - V(E)\mathcal{G}^0_{0,0}}\mathcal{G}^0_{0,0}\mathcal{G}^0_{0,0} \\ &= \frac{\mathcal{G}^0_{0,0}}{1 - V(E)\mathcal{G}^0_{0,0}} \quad .\end{aligned} \tag{4.46}$$

The only remaining task is to find the function $V(E) = V_0 + V_{eff}(E)$, with $V_{eff}(E) = V^{\uparrow}_{eff}(E) + V^{\downarrow}_{eff}(E)$. Let us begin with $V^{\uparrow}_{eff}(E)$ defined in Eq.(4.36):

$$\begin{aligned}V^{\uparrow}_{eff}(E) &= \frac{1}{4}V_1^2 < 0|\frac{1}{\mathcal{C}(E+1) - V^{\uparrow}_{eff}(E+1)\ |0><0|}|0> \\ &= \frac{1}{4}V_1^2 < 0|\frac{1}{(\mathcal{G}^0(E+1))^{-1} - (V_0 + V^{\uparrow}_{eff}(E+1))|0><0|}|0> \\ &= \frac{1}{4}V_1^2 < 0|\frac{\mathcal{G}^0(E+1)}{1 - (V_0 + V^{\uparrow}_{eff}(E+1))|0><0|\mathcal{G}^0(E+1)}|0>\end{aligned} \tag{4.47}$$

this last expression, following the procedure beginning with Eq.(4.41) is easily found to give a result very similar to Eq.(4.46),

$$\begin{aligned}V^{\uparrow}_{eff}(E) &= \frac{1}{4}V_1^2\frac{\mathcal{G}^0_{0,0}(E+1)}{\mathtt{1} - (V_0 + V^{\uparrow}_{eff}(E+1))\mathcal{G}^0_{0,0}(E+1)} \\ &= \frac{\frac{1}{4}V_1^2}{(1/\mathcal{G}^0_{0,0}(E+1) - V_0) - V^{\uparrow}_{eff}(E+1)} \quad .\end{aligned} \tag{4.48}$$

Iterating this equation we get the final expression

$$V_{eff}^{\uparrow}(E) = \cfrac{\frac{1}{4}V_1^2}{(1/\mathcal{G}_{0,0}^0(E+1) - V_0) - \cfrac{\frac{1}{4}V_1^2}{(1/\mathcal{G}_{0,0}^0(E+2) - V_0) - \cfrac{\frac{1}{4}V_1^2}{\vdots}}} \quad . \tag{4.49}$$

Similarly for $V_{eff}^{\downarrow}(E)$ we find

$$V_{eff}^{\downarrow}(E) = \cfrac{\frac{1}{4}V_1^2}{(1/\mathcal{G}_{0,0}^0(E-1) - V_0) - \cfrac{\frac{1}{4}V_1^2}{(1/\mathcal{G}_{0,0}^0(E-2) - V_0) - \cfrac{\frac{1}{4}V_1^2}{\vdots}}} \quad . \tag{4.50}$$

For the $\mathcal{H}^0$ given in Eq.(4.33) it is well know that $1/\mathcal{G}_{0,0}^0(E) = \pm\sqrt{E^2 - 4T^2}$ (the sign choice will be discussed later). With this, the Floquet-Green's function for the system in Eq.(4.32) is completely solved in terms of the parameters (T, V_0, V_1, E). Explicitly,

$$\mathcal{G}_{0,0}^D(E) = \cfrac{2/V_1}{a(E) - \cfrac{2}{V_1}V_{eff}(E)} \quad , \tag{4.51}$$

where

$$V_{eff}(E) = \cfrac{V_1/2}{a(E+1) - \cfrac{1}{a(E+2) - \cfrac{1}{\vdots}}} + \cfrac{V_1/2}{a(E-1) - \cfrac{1}{a(E-2) - \cfrac{1}{\vdots}}} \quad , \tag{4.52}$$

and, to simplify notation we defined the function

$$a(E) = \pm\frac{2\sqrt{E^2 - 4T^2}}{V_1} - 2\frac{V_0}{V_1} \quad . \tag{4.53}$$

The choice in the sign of the function $\pm\sqrt{E^2-4T^2}$ is not a trivial one. For a system with perfect spacial periodicity it is irrelevant; however, our system does not have such periodicity; the presence of the defect potential does force a choice in the sign. One can show that $\mathcal{G}^D_{0,i} = \mathcal{G}^D_{0,0}R(E)^{|i|}_{\pm}$. Where $R_{\pm}(E) = \frac{E}{2T} \pm \sqrt{(E/2T)^2-1}$. When $E > 2T > 0$, $R_+ > 1$ and $R_- < 1$. The first choice (+) is not physical since it gives a Green's function that diverges in space; this force us to chose the negative sign for the square root in the case $E > 2T > 0$. A similar analysis shows that for $E < -2T < 0$, the plus sign in the square root is required. This sign change can be accomplished if we replace $\sqrt{(E/2T)^2-1}$ by $(E/2T)\sqrt{1-(2T/E)^2}$. Using this, the correct form for Eq.(4.53) is

$$a(E) = \frac{2E}{V_1}\sqrt{1-\left(\frac{2T}{E}\right)^2} - 2\frac{V_0}{V_1} \quad . \tag{4.54}$$

It could be argued that one does not have to bother taking care of the proper sign in $\mathcal{G}^0_{0,0}$ for $|E| > 2T$ because that is outside of the band $-2T < E < 2T$ where there might not even be any states. This is not true because of the possible existence of bound states outside of the band (which is clearly the case for $V_0 \neq 0$,$V_1 = 0$). Another argument is that some of the off diagonal (in Floquet index) elements of the Floquet-Green's function will necessarily have energies outside of the band, i.e., if $E = \alpha\hbar\omega$ is inside the band, $E + n\hbar\omega$ is obviously not necessarily in it, and therefore, the matrix elements $\mathcal{G}_{\alpha+n,\alpha}(0,j) = \mathcal{G}_{\alpha+n,\alpha}(0,0)(1/R^{\uparrow}(E+n))^j$ when $|E+n\hbar\omega| > 2T$ will not converge as $j \to \infty$ unless the previously mentioned selection of sign is

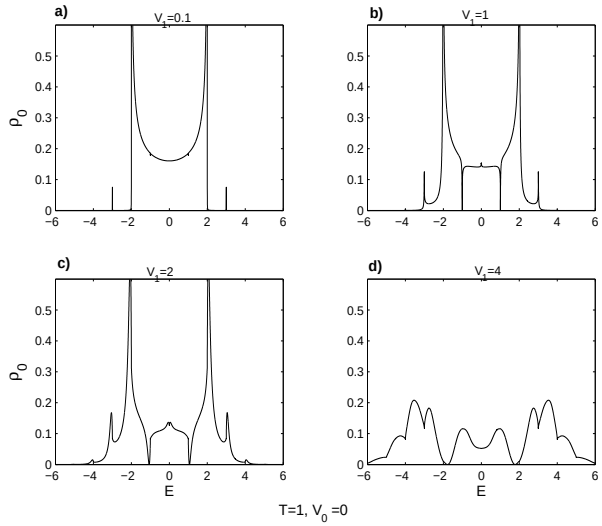

Figure 4.1: LDOS for a tight binding Hamiltonian with a defect energy oscillating in time. $T = 1, V_0 = 0$ (units of $\hbar\omega$) . The width of the band (4T) is bigger than $\hbar\omega$.

made for $a(E + n\hbar\omega)$.

The LDOS at the defect location can be calculated from the diagonal elements of the Green's function with the usual formula,

$$\rho_0(E) = \mp\frac{1}{\pi} Im(\mathcal{G}^D_{0,0}(E \pm i\gamma)) \tag{4.55}$$

In the derivation of this equation, which relates the density of states with the Green's function, it is necessary to include $\pm i\gamma$ in the energy to get the contribution, in the density of states, of the discrete part of the spectrum (poles). In our numerical calculations, $\gamma = 10^{-7}$ unless otherwise specified.

Fig.4.1 shows a plot of $\rho_0(E)$, for different values of V_1, where all parameters are given in units of $\hbar\omega$, and $V_0 = 0, T = 1$. In a) it can be seen

that the LDOS is very close to the expected LDOS for the static part of the hamiltonian($\mathcal{H}^0$), with the allowed energy band located between $-2T$ and $2T$. As the value of V_1 is increased one can see some of the eigenstates leaking out of the band and populating the region outside the interval $[-2, 2]$. The first ones to do so are the unperturbed eigenstates in "resonance" with the oscillating potential; that is the ones with energy close to $\pm\hbar\omega$. For $V_1 = 2$ the distribution is even broader with the features of the unperturbed hamiltonian still recognizable. At $V_1 = 4$ the density of states has significantly spread over the region $-6 < E < 6$. For no value of V_1 do we find any poles (localized states) in the system.

Figure 4.2 shows the LDOS for $T = 1$, $V_0 = 1$ and various values of V_1. For a very small V_1 we see the LDOS expected for a tight-binding model with an impurity, where the impurity produces a localized state (pole in the density of states) at an energy $sign(V_0)\sqrt{4T^2 + {V_0}^2}$. A "pole" can be seen in a) at the expected value $\sqrt{4T^2 + {V_0}^2} = \sqrt{5}$. Closer analysis of this peak near $\sqrt{5}$ reveals that this is actually not a true pole. If this peak in the LDOS were truly a pole, its height should be proportional to $1/\gamma$ and therefore it should go to infinity as $\gamma \to 0$. For all the values of V_1 shown in Fig. 4.2, the height of the peak eventually saturates as γ is made smaller. For $V_1 = 0.0001$ the height as a function of γ saturates for $\gamma = 10^{-11}$; for $V_1 = 0.01$ we get a $\gamma \sim 10^{-7}$. For bigger values of V_1 saturation occurs for even smaller values of γ. This implies that the bound state of the static potential, in the presence of the oscillating potential, acquires a finite life time and therefore on can say

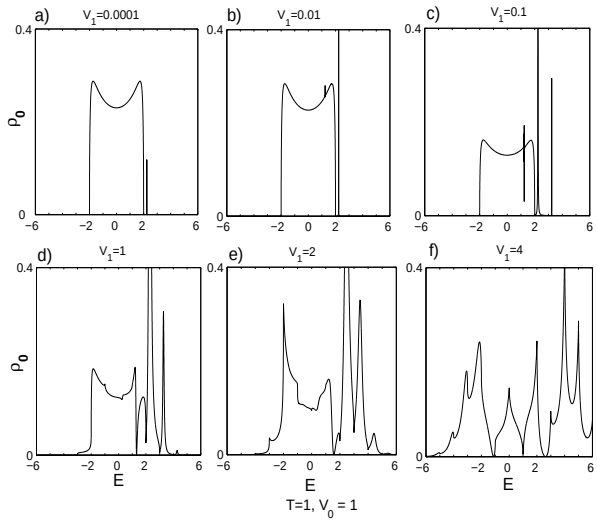

Figure 4.2: LDOS for different values of the amplitude of the oscillation. As in Fig.4.1, $T = 1$ and the defect has a static on-site energy $V_0 = 1$. No poles where obtained at any value of V_1.

that the oscillating potential "ionizes" the bound state of the static part of the Hamiltonian.

It has been shown before [51] that, for an attractive δ-function potential, the addition of a time-periodic perturbation in the strength of the δ-function always "ionizes" the bound state. It is actually easy to understand why it is so. The time-periodic perturbation couples the unperturbed Hamiltonian's bound state, with energy E_B, with all the unperturbed states at energies $E_B + n$ (in units of $\hbar\omega$). Clearly, for any E_B there is a value of n above which the unperturbed states will be in the continuum ($E_B + n > 0$). That means that the bound state has a finite probability to transition into those states and escape. Because of this, the resonance associated with it has an intrinsic

non-zero width given by the inverse of the life time. In our case, in addition to the localized time-independent potential (the V_0 part of the defect energy) we have the tight-binding hamiltonian, which does not have a continuum at high energies. Its continuum lies only in the interval [-2T, 2T]. Despite this, the argument that justifies the absence of a bound state applies almost the same: If the width of the energy band of $\mathcal{H}^0$ ($4T$) is greater than 1 ($\hbar\omega$), no matter what is the energy of the bound state (E_B) associated with V_0, there will be at least one energy $E_B + n$ (for some n) that will fall inside the extended states band (the continuum). The bound state of the time independent Hamiltonian, due to the time-harmonic potential, is therefore coupled to at least one extended state and therefore becomes no longer bound (for $4T > 1$). For small values of V_1, these kind of narrow resonances associated with bound states are called quasi-bound states and are typical of multichannel Hamiltonians [26]. At $V_1 = 0.1$ it is interesting to notice the "daughter" resonances on both sides of the bound state resonance at $\sqrt{5} \pm 1$. In fact there is an infinite number of these "daughter" resonances at $\sqrt{5} + n$ with an amplitude that decays quickly with $|n|$. For large values of V_1, a complex structure of peaks have developed, being separated in energy by integer values of $\hbar\omega$. This is what would be expected if instead of a HD potential we had a harmonic oscillator coupled to the electron. For large coupling (V_1), the density of states of the oscillator becomes dominant in the LDOS of the electron.

In Fig.4.3 we study an interesting regime. For $T = 0.1$, the width ofthe energy band of $\mathcal{H}^0$ ($4T = 0.4$) is smaller than 1. In this figure, $V_0 = 0$, and

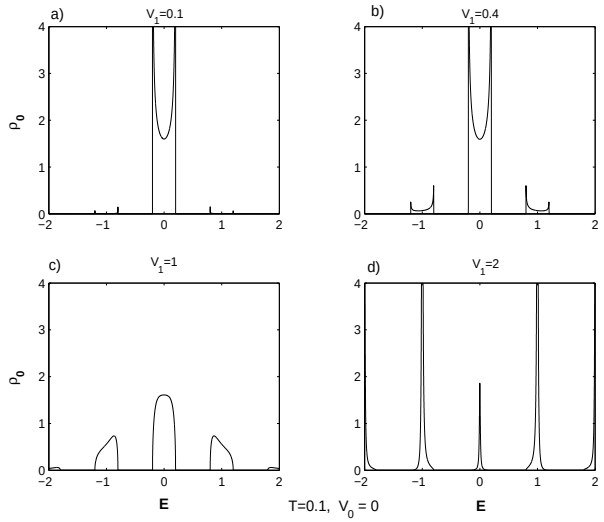

Figure 4.3: LDOS for a small band width. $T = 0.1(\hbar\omega)$, and therefore, the width of the band (4T) is smaller than $\hbar\omega$. No static on-site energy, $V_0 = 0$.

we look at different values of V_1. In a) the density of states is very close to the well known LDOS for a tight binding model without a defect. Very small replica bands can be observed around $E = \pm 1$. In b) these replica bands are more noticeable. For $V_1 = 1$ in c), the shape of the LDOS inside the bands is starting to change. For $V_1 = 2$ and higher, the LDOS looks very much like the LDOS for a harmonic oscillator, highly peaked around $E = n(\hbar\omega)$.

For Fig.4.4 we chose again $T = 0.1$, and $V_0 = 0.1$. This gives an energy of the bound state of $\mathcal{H}^S$ of $E_B = \sqrt{0.04 + .01} = 0.2236$. Because the band width is smaller than 1, the bound state is coupled to unperturbed states with energies $E_B + n$ which are all outside the extended states band. This means one would expect that, for small V_1, as in Fig.4.4(a), there will be a true pole in the density of states at an energy $E_B \sim 0.223$. Indeed, within our

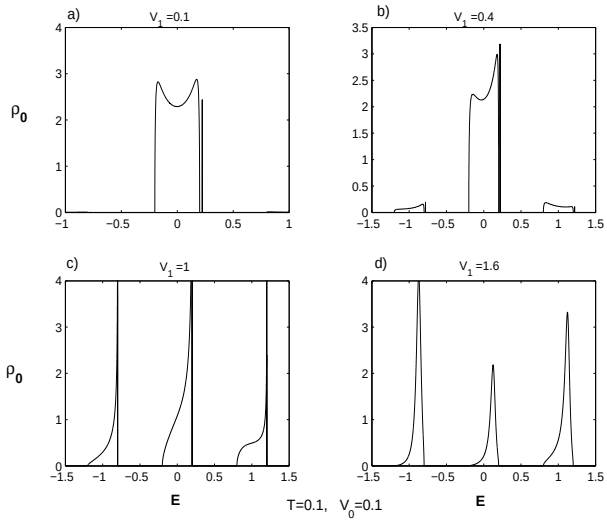

Figure 4.4: LDOS for $T = 0.1$, $V_0 = 0.1$ and different values of V_1. There is a pole on the right of the extended states band for $V_1 < 1$.

numerical possibilities, no saturation in the height of the peak was detected when decreasing γ. In (b), $V_1 = 0.4$. We still have a pole on the right of the band, but its energy is down to $E_B = 0.2185$. The pole moves towards the extended states band as we increase V_1. Notice that there are replica bands of extended states centered around $E = n$, as well as replica poles (too small to be seen in Fig.4.3. In (c), for $V_1 = 1.0$ there is still a pole, located right next to the edge of the band. In the figure, this pole is too close to be discernible from the edge of the continuum of extended states. At $V_1 = 1.6$ in (d), the pole has already disappeared inside the band; there are no longer localized states in the system and the spectrum of the system resembles the spectrum of the harmonic oscillator, with density of states highly peaked near $E = 0.1 + n$.

In Fig.4.5 we show a sequence of plots where $T = 0.1, V_0 = 0.4$ for

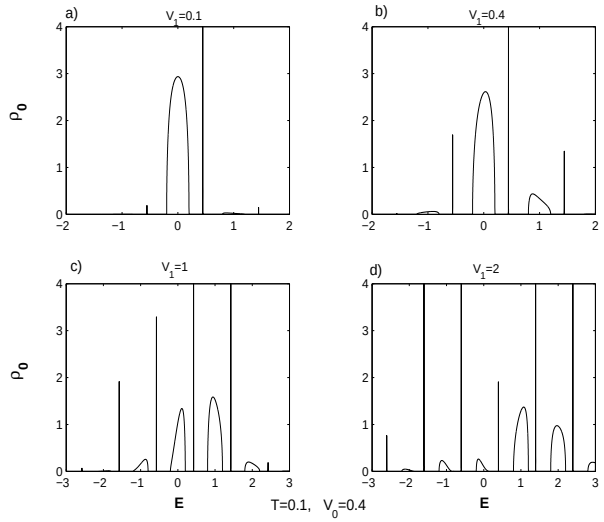

Figure 4.5: LDOS for $T = 0.1$, $V_0 = 0.4$ and different values of V_1. There are poles for all values of V_1. Pole location changes from 0.44 +n for $V_1 \to 0$ to $\sim 0.4 + n$ for $V_1 \to \infty$, with n any integer.

different values of V_1. In a), $V_1 = 0.1$, and we find a pole very close to $E_B = \sqrt{4T^2 + V_0^2} = 0.447$, which is the location of the pole for the static potential case ($V_1 = 0$). For $V_1 = 0.4$ in Fig.4.5(b), the pole has moved to $E_B \sim 0.443$ and the "replica bands" are clearly seen on the right and left of the main band (near $E = 0$). Also two "daughter" poles are big enough to be seen at $E = 0.443 \pm 1$. In (c) $V_1 = 1$, the poles have moved to $E = 0.424 + n\hbar\omega$, and the relative amplitude of the continuum part of the spectrum is growing smaller compared to the set of localized states (poles), for increasing V_1 values. The extension of the region where poles have significant residue to be observable in the figure grows with V_1. For (d) $V_1 = 2$, the poles are now at $E \sim 0.3955 + n$. As the value of V_1 is increased further, the pole does not move anymore from

this location and the point spectrum (poles) becomes more and more important as compared to the continuum spectrum. For all values of V_1, for $T = 0.1$ and $V_0 = 0.4$ there is a pole.

It can be proven easily that the location of the poles behave in the following way for any values of V_0, V_1 and T (provided $4T < 1(\hbar\omega)$):

$$E_B \rightarrow \sqrt{4T^2 + V_0^2}+n \ \text{ for } \mathrm{V_1} \rightarrow 0 \ , \qquad \mathrm{E_B} \rightarrow \mathrm{V_0}+\mathrm{n} \ \text{ for } \mathrm{V_1} \rightarrow \infty. \quad (4.56)$$

There would not be a pole in any of these limits if the expected location of the pole (in this limit) falls inside the extended states band between $-2T, 2T$. This is the case in Fig. 4.4 ($T = 0.1$, $V_0 = 0.1$), where, when $V_1 \rightarrow 0$, pole location $\rightarrow\sqrt{4T^2 + V_0^2} = 0.223$ and for $V_1 \rightarrow \infty$, expected "pole" location $\rightarrow V_0 = 0.1$, which is inside the band. Already for $V_1 > 1$ the pole has moved into that band (it is no longer a pole), generating a peak in the density of states, which continues to move inside the band for increasing values of V_1 until it settles at $E = V_0 + n \sim 0.1 + n$ for $V_1 > 2$.

Chapter 5

Conclusions

In chapter 2 we found an exact solution for the problem of transmission of a particle through a monochromatic oscillating potential through the use of C.F's. Apart from the short computational time as compared to numerical diagonalization, continued fractions allowed us to prove rigorously general properties of the transmission for this system, such as the existence of transmission zeros only for incoming energies smaller than $\hbar\omega$.

We also found that in the complex plane the system has an infinite number of poles (resonances) located at regular intervals of $\hbar\omega$ in the incident energy. The scattering matrix and any quantity related to it has a very complex structure in the complex energy plane due to the different channel-momentum factors (square roots) which appear in it, creating in principle an infinitely sheeted structure. From this multitude of sheets however, only the ones that are a smooth analytic continuation of the real energy axis have relevance. It is in those sheets that the poles can be found. As expected, the residue of these poles decreases with increasing energy.

Because of the unitarity of the S-matrix, it is known that a pole must always be accompanied by a zero which may or may not occur in the real

energy axis. Only for incident energies smaller than $\hbar\omega$ and for certain ranges in the strength of the oscillation we find the zero to be located on the real energy axis. This zero in the transmission is indeed an interesting feature, since no static potential (except for an infinite wall) could reflect completely an incoming particle. It is also only in those same ranges of the strength of the oscillation were the S-matrix has poles (because of the unitarity condition). We found 'threshold anomalies' in the transmission probability (its derivative diverges) at the channel openings, which are due to the square root dependence on energy of the S-matrix elements.

Even though these scattering properties have been found for a particular case of harmonically driven system (delta-function potential), we believe that in most cases the reasons behind their occurrence is sufficiently general for us to expect them to occur in other situations where the potential is also localized and harmonically dependent on time.

In chapter 3 we studied another kind of harmonically driven potential, an infinite chain of harmonically driven delta oscillators. For this purpose we used two basic methods: degenerate perturbation theory and Floquet translation matrix. Degenerate perturbation theory was developed to give a more physical picture for the avoided crossings in the perturbative regime. The translation matrix method was developed as a more efficient method to calculate the eigenstates of the system. Transfer matrix or translation matrix (TM) methods have been used before in extended systems but rarely in multichannel problems. The advantage in using such method is quite important:

the construction of the translation-by-a-period matrix operator requires solving Schrodinger's equation only in one cell of the infinite periodic potential. A study of the TM eigenvectors and eigenvalues provides the eigenstates and dispersion relations for the quantum numbers of the allowed states of the infinite system.

Due to the simple structure of the translation matrix we were also able to find its eigenvectors using continued fractions, which proved important in understanding the contribution to the eigenstates of the infinite chain due to the evanescent modes, also, turns out to be the only way to include their effect for parameters of the system that give a small effective $\hbar$;for , in this regime, these exponential modes destroy the accuracy of any numerical diagonalization of the TM matrix.

We showed that the quasi-bound states (resonances in the S-matrix) of a single delta contribute significantly to the structure of the low energy Floquet-Bloch states of the chain. These bands can therefore be considered the 'quasi-bound state bands' of the system. Oscillating deltas are therefore "sticky" in the sense that the wave-function (at low energies) tends to stick around in the neighborhood of the delta. This tendency to do so is related to the existence (for complex energies) of quasi-bound states which in the real energy axis manifest themselves as resonances; they can be thought of as incoming states that are trapped inside the scattering region for some finite time (Wigner delay time).

Analysis of the average-energy of the eigenstates of the system when

a harmonic (frequency ω) perturbation is present reveals an interesting effect when the energy of the unperturbed system is close to a multiple of $\hbar\omega$. Turning on the harmonic space-periodic potential might cause the particle to give away all its energy.

We studied the dynamics of the quasi-energy band structure as a function of the strength of a time periodic potential and found that the lowest (in average energy) bands are strongly affected by this parameter. They show an almost periodic dependence on the square of the oscillator strength, with successive exchanges of identity between these bands. This is consistent with the fact, mentioned in chapter 2, that the pole location (quasi-bound state energy) seems to change also in an almost periodical way with the square of the strength of the oscillating delta. Since the quasi-bound state has a very important presence in those lowest energy bands, one would expect them to change accordingly with this parameter.

We identified points in the quasi-energy band structure related with standing waves whose nodes correspond to the location of the oscillating δ-functions in the chain. At these points (at the edge and center of the momentum Brillouin zone) one of the bands that participate in an avoided crossing remains pinned as the strength of the oscillating potential is changed (the band whose corresponding eigenfunction is antisymmetrical). This effect, although theoretically possible has no counterpart in any real situation since it depends critically on the potential having no spatial extension; any potential with a range different from zero would not leave this states 'untouched'.

We found that for certain values of the strength of the oscillating potential, the width of one of the Q.E. bands becomes very small. This phenomenon has been called in the literature 'band collapse'. It provides a possible mechanism to produce highly non-dispersive (coherent) states in a waveguide or super-lattice. We found that the 'collapse' is related to the dynamical quenching of the transmission through a single oscillating δ-function potential.

In chapter 4 we make use of what is the common mathematical feature of all time-harmonic potentials: the Hamiltonian couples only states that are nearest-neighbors in energy (E with $E + \hbar\omega$ and $E - \hbar\omega$). This simple fact means that in principle all thess potentials could be solved using the same basic method that we developed in chapter 2 for the solution of a three term recursion relation in the coefficients of the wave-function. Using this technique, we developed a general method to calculate the Floquet-Green's function of this kind of systems.

Once the Floquet-Green's function of a system is known, all its transmission properties can be calculated as well as density of states, wave packet propagation,etc. We showed that in the general case of harmonic driving, the Floquet-Green's function of any such system can be written in a compact way and be calculated efficiently using Matrix continued fractions (MCF). Traditional approaches to the problem of a system under harmonic drive have relied on perturbative or approximate treatments such as the rotating wave approximation(RWA) which break down for strong amplitudes of the driving field. Our procedure for the calculation of the Floquet-Green's function can be used

to reach any degree of accuracy at any strength of the driving field. A truncation of the MCF to only one step does already include the contribution to the Floquet-Green's function of an infinite number of terms in its perturbation expansion.

We also derived an expression for the (energy dependent) dynamical effective potential (D.E.P.) which includes the effect of the coupling to the different energy states due to the time periodicity of the system. This quantity is equivalent to the calculation, in a time-independent system, of the 'self-energy' which is due to the coupling between, for example, a cavity and the leads. The D.E.P. allows one to calculate the diagonal of the Floquet-Green's function operator from which the density of states can be found easily. Calculation of the D.E.P could provide an interesting tool to help understand effects such as dynamical stabilization of atoms in a strong laser field.[50]

We applied this formalism to the case of a tight-binding model with a defect energy which depends harmonically on time. The transmission through this defect potential has been calculated before and compared to the transmission through a tight-binding Hamiltonian with a defect that couples the electron with phonon degrees of freedom only present at the defect location.[54] We calculated the diagonal of the Floquet-Green's function at the defect location ($G^D_{0,0}$) and from it, the LDOS as a function of energy for different values of the parameters of the system. We found that there is a qualitative difference in the behavior of the system for the regimes $4T > \hbar\omega$ and $4T < \hbar\omega$. In both cases we found that the LDOS spreads over a bigger range of energies as

the parameter V_1 is increased. However, in the first case there are no localized states for any values of the parameters V_0,V_1. This result is due to the fact that the oscillating potential couples the bound state with at least one extended state of the unperturbed Hamiltonian, producing a finite probability of scape from the bound state. Turning on the oscillating potential will therefore, in all cases (provided $4T > \hbar\omega$), "ionize" the bound state (if any) of the static part of the Hamiltonian. This result is consistent with the work of Costin et al.[51] which shows that the bound state of an attractive δ-function potential does not remain bound when a time-periodic driving is turned on (except for a very particular class of non-harmonic periodic driving). For the case $4T < \hbar\omega$, there may or may not be any localized states in the system depending on the different values of V_0 and V_1. A bound state outside of the band can only be coupled to energy eigenstates of the static hamiltonian which are all localized. The effect of the oscillating potential changes the location of the localized states energy, and produces an infinite chain of poles in the LDOS, all located at multiples of $\hbar\omega$ from each other. The pole location changes with the parameter V_1 according to Eq.(4.56). In both cases ($4T > \hbar\omega$ and $4T < \hbar\omega$), the LDOS transitions from the LDOS of the static defect problem, for small V_1, to a harmonic-oscillator-like LDOS for V_1 large.

The problem of harmonic driving in a quantum system is an old and important one. In this work we have studied numerically and analytically simple but interesting problems that we believe increased significantly the understanding of the effects of this type of driving, and we have also developed

an important tool (Floquet-Green's function in terms of MCF) that can be used to investigate the dynamics of any harmonically driven quantum system.

Appendices

Appendix A

Ratio of the elastic transmission amplitudes

For a single oscillating delta-function potential, it has been shown[42] that the elastic transmission amplitude C_n obeys an equation of the form

$$C_n = \frac{1}{F_n + G_n} \tag{A.1}$$

with

$$F_n(\epsilon) = 1 + \frac{h_n^2(\epsilon)}{F_{n+1}(\epsilon)} \quad , \tag{A.2}$$

and

$$G_n(\epsilon) = \frac{h_{n-1}^2(\epsilon)}{1 + G_{n-1}(\epsilon)} \quad . \tag{A.3}$$

Therefore,

$$\frac{C_{-n}}{C_{-n+1}} = \frac{F_{-n+1}}{1 + G_{-n}} \quad . \tag{A.4}$$

When this expression is evaluated at the value of the quasi-energy for which the S-matrix has poles on each channel, we obtain (*indicates that the corresponding function is evaluated at the pole) $F^*_{-n+1} = -G^*_{-n+1}$, and therefore,

$$\frac{C^*_{-n}}{C^*_{-n+1}} = \frac{F^*_{-n+1}}{1 + G^*_{-n}} = -\frac{G^*_{-n+1}}{1 + G^*_{-n}} = -\frac{h^{2*}_{-n}}{(1 + G^*_{-n})^2} = -Z^{*2}_{-n} \quad . \tag{A.5}$$

Appendix B

S-matrix and quasi-bound states

A quasi-bound state associated with the pole of an S-matrix can be found using the following argument. In general, any complex symmetric matrix, for example the S-matrix in the complex plane, with n distinct eigenvalues can be written in the form [48]

$$\mathbf{S} = \mathbf{V} D \mathbf{V}^T, \tag{B.1}$$

where D is a diagonal matrix. This can be written as

$$\mathbf{S} = \alpha_1 \mathbf{V}_1 \wedge \mathbf{V}_1^T + \alpha_2 \mathbf{V}_2 \wedge \mathbf{V}_2^T + ... \ , \tag{B.2}$$

where $\alpha_1, \alpha_2, ..$ are the diagonal elements of $\mathbf{D}$ (which are proportional to the eigenvalues of S) and $\mathbf{V_1}, \mathbf{V_2}, ...$ are the columns of $\mathbf{V}$. As we approach a pole of the S-matrix, $E \to E^*$, and one of the eigenvalues of $\mathbf{S}$ diverges. Therefore, $S \to S^*$, where

$$S^* = \alpha \mathbf{V}_{_{QB}} \wedge \mathbf{V}_{_{QB}}^T, \qquad \text{with} \ \ \alpha \to \infty \quad \text{as} \quad \mathrm{E} \to \mathrm{E}^*. \tag{B.3}$$

$\mathbf{V_{QB}}$ is the quasi-bound state, and it does not correspond to a square integrable wave-function. We define it as the eigenvector of S whose eigenvalue diverges at the pole. Now we proceed to show, using the exact solution for the S-matrix

of the single δ-function potential that, at the pole location, $\mathbf{S}$ can be written in this way and we will find the corresponding components of $\mathbf{V_{QB}}$.

The diagonal elements of the transmission matrix are given by the quantities C_n. From this diagonal one can produce the rest of this matrix by using the functions f_n as defined in [42]. The S-matrix (near the pole) can be written as (only the transmission components are shown)

$$\mathbf{S}^* = \begin{pmatrix} \ddots & \vdots & \vdots & \vdots & \vdots & \\ \dots & 1 & 1/Z^*_{-1} & 1/(Z^*_{-1}Z^*_{-2}) & 1/(Z^*_{-1}Z^*_{-2}Z^*_{-3}) & \dots \\ \dots & Z^*_{-1} & 1 & 1/Z^*_{-2} & 1/(Z^*_{-3}Z^*_{-2}) & \dots \\ \dots & Z^*_{-1}Z^*_{-2} & Z^*_{-2} & 1 & 1/Z^*_{-3} & \dots \\ \dots & Z^*_{-1}Z^*_{-2}Z^*_{-3} & Z^*_{-2}Z^*_{-3} & Z^*_{-3} & 1 & \dots \\ & \vdots & \vdots & \vdots & \vdots & \ddots \end{pmatrix} D \quad , \tag{B.4}$$

with D a diagonal matrix with diagonal elements $D = (.....C^*_0, C^*_{-1}, C^*_{-2}.....)$. In the above expression we made use of the fact that to go down on a column starting from the diagonal matrix multiplies by Z^*_n, and to go up on a column from the diagonal matrix element divides by Z^*_n (this is only true at the pole, where $F^*_n = -G^*_n$). From this, using $D = C^*_0(...1, Z^{*2}_{-1}, Z^{*2}_{-1}Z^{*2}_{-2}, Z^{*2}_{-1}Z^{*2}_{-2}Z^{*2}_{-3}...)$, we write $\mathbf{S}^*$ as

$$\mathbf{S}^* = C^*_0 \begin{pmatrix} \ddots & \vdots & \vdots & \vdots & \\ \dots & 1 & Z^*_{-1} & Z^*_{-1}Z^*_{-2} & \dots \\ \dots & (Z^*_{-1}) & Z^*_{-1}(Z^*_{-1}) & Z^*_{-1}Z^*_{-2}(Z^*_{-1}) & \dots \\ \dots & (Z^*_{-1}Z^*_{-2}) & Z^*_{-1}(Z^*_{-1}Z^*_{-2}) & Z^*_{-1}Z^*_{-2}(Z^*_{-1}Z^*_{-2}) & \dots \\ \dots & (Z^*_{-1}Z^*_{-2}Z^*_{-3}) & Z^*_{-1}(Z^*_{-1}Z^*_{-2}Z^*_{-3}) & Z^*_{-1}Z^*_{-2}(Z^*_{-1}Z^*_{-2}Z^*_{-3}) & \dots \\ & \vdots & \vdots & \vdots & \ddots \end{pmatrix} . \tag{B.5}$$

This expression has exactly the form anticipated in the discussion about the form of the S matrix near the pole, since it can be written as an external product,

$$\mathbf{S}^* = C_0^* \mathbf{V}_{QB} \wedge \mathbf{V}_{QB}^T \quad , \tag{B.6}$$

with

$$\mathbf{V}_{QB}^T = (....., 1, Z_{-1}^*, Z_{-1}^* Z_{-2}^*, Z_{-1}^* Z_{-2}^* Z_{-3}^*, ...) \quad , \tag{B.7}$$

and ${C_0}^*$ diverging at the pole.

Bibliography

[1] G.W. Hill, Acta Mathematica, Vol.8, 1, 1877

[2] V. Zanchin, A. Maia, W. Craig and R. Brandenberger, Phys. Rev. D, 57, 4651(1998).

[3] G. Floquet, C.R. Acad. Sci. Paris, 91, 880(1880); G. Floquet, Ann. Sci. École Norm. Sup., 12, 47(1883).

[4] F. Bloch, Z. Phys. 52, 555, 1928.

[5] J.H. Shirley, Phys. Rev. B, 138, 979 (1965).

[6] H. Sambe, Phys.Rev.A, 7, 2203(1972).

[7] S.C. Althorpe, D.J. Kouri, D.K. Hoffman, N. Moiseyev, Chem.Phys., 217, 289(1997); U. Peskin, N. Moiseyev, J.Chem.Phys, 99, 4590(1993).

[8] C. Brezinsky in *History of Continued Fractions and Paé Approximants*, from the Springer series in Computational Mathematics, (Springer-Verlag, Berlin,1991).

[9] B. Kónya, G. Lévai, Z. Papp, J.Math.Phys., 38, 4832(1997).

[10] S.G. Davison, R.A. English, Z.L. Miskovič, F.O. Goodman, A.T. Amos, and B.L. Burrows, J.Phys.-Cond.Mat. 9, 6371(1997).

[11] J.P. Vigneron, Ph. Lambin, J. Phys.A: Math. Gen. 13, 1135(1980).

[12] S.H. Autler, C.H. Townes, Phys.Rev., 100, 703(1955).

[13] K. Berg-Sorenson, Y. Castin, E. Bonderup, K. Molmer, J.Phys.B, 25, 4195(1992).

[14] B.Y. Gelfand, S. Schmitt-Rink, A.F.J. Levi, Phys.Rev.Lett., 62, 1683(1989).

[15] L.E. Reichl in *The Transition to Chaos in Conservative Classical Systems: Quantum Manifestations*, (Springer-Verlag, New York, 1992).

[16] M. Büttiker, R. Landauer, Phys.Rev.Lett., 49, 1739(1982).

[17] J.A. Stovneng, E.H. Hauge, J.Stat.Phys., 57, 841(1989).

[18] T. Tanizawa, J.Phys.Soc.Japan, 65, 3157(1996).

[19] F. Bench,H.J. Korsch, N. Moiseyev, J.Phys.B, 24, 1321(1991).

[20] O. Costin, J.L. Lebowitz, A. Rokhlenko, J.Phys.A, 33, 6311(2000).

[21] P.F. Bagwell, R.K. Lake, Phys.Rev.B, 46, 15329(1992).

[22] E. Cota, J.V. Jose, F.Rojas, Nanostructured Materials, 3, 349(1993).

[23] W. Li, L.E. Reichl, Phys.Rev.B, 60, 15732(1999).

[24] M. Wagner, Phys.Rev.A, 51, 798(1995).

[25] K.W. McVoy in *Fundamentals in Nuclear Theory*, edited by A. De-Shalit and C. Villi, (International Atomic Agency, Vienna, 1967).

[26] P.F. Bagwell, A. Kumar, R.K. Lake in *Quantum Effect Physics, Electronics and applications*, edited by K. Ismail et al., (Adam-Hilger, Bristol, 1992).

[27] D.S. Saraga, M. Sassoli-de-Bianchi, Helv.Phys.Acta, 70, 751(1997).

[28] R.G. Newton in *Scattering theory of waves and particles*, (McGraw-Hill, New York, 1966).

[29] For a good review, see E.E. Mendez and Gerald Bastard, Phys. Today 46, No.6, 34 (1993).

[30] M. Holthaus, Phys. Rev. Lett. 69, 351 (1992); M. Holthaus and D. Hone, Phys. Rev. B 47, 6499 (1993); M. Holthaus and D. Hone, Phys. Rev. B 49,16605 (1994);K. Drese and M. Holthaus, J.Phys.:Condens.Matter 8, 1193 (1996).

[31] D.H. Dunlap and V.M. Krenke, Phys. Rev. B 34, 3625 (1986); Phys.Lett. A 127,438 (1988); S. Raghavan, V.M. Kenkre, D.H. Dunlap, A.R. Bishop, M.I. Salkola, Phys. Rev. A, 54, 1781 (1996).

[32] B.J. Keay, S.J. Allen Jr., J. Galán, J.P. Kaminsky, K.L. Campman, A.C. Gossard, U. Bhanttacharya, and M.J.W. Rodwell, Phys. Rev. Lett. 75, 4098 (1995); B.J. Keay, S. Zeuner, and S.J. Allen,Jr., K.D. Maranowski, A.C. Gossard, U. Bhattacharya, M.J.W. Rodwell, Phys. Rev. Lett. 75, 4102 (1995).

[33] H. Schanz, M.F. Otto, R. Ketzmerick and T. Dittrich, Phys. Rev. Lett. 87, 70601 (2001).

[34] I. Goychuk and P. Hänggi, in *Lecture notes on Physics*, edited by J. Freund and T. Pöschel (Springer, Berlin, 2000), Vol. 557, pp. 7-20.

[35] R. Roncaglia, L. Bonci, F.M Izrailev, B.J West and P. Grigolini, Phys. Rev. Lett. 73, 802 (1995).

[36] R. Utermann, T. Dittrich and P. Hänggi, Phys. Rev. E 49, 273 (1994).

[37] O. Bohigas, S. Tomsovic and D. Ullmo, Phys. Rep. 223, 43 (1993).

[38] D.A. Steck, W.H. Oskay, and M.G. Raizen, Science 293, 274 (2001).

[39] W.K. Hensinger, H. Häffner, A. Browaeys,N.R. Heckenberg,K. Helmerson, C. McKenzie, G.J. Milburn, W.D. Phillips, S.L. Rolston, H. Rubinsztein-Dunlop and B. Upcroft, Nature 412, 52 (2001).

[40] D.J. Thouless, Phys. Rev. B 27, 6083 (1983).

[41] J. H. Hannay and R.J. McCraw, J.Phys. A: Math. Gen. 23, 887 (1990).

[42] D.F.Martinez, L.E.Reichl, Phys. Rev. B, 64, 245315 (2001).

[43] J. von Neumann and E. Wigner, Phys. Z. 30, 467 (1929), translated in R.S. Knox and A. Gold, Symmetry in the Solid State (Benjamin, New York, 1964).

[44] E.M. Zanardy and J.M Gomez Llorente, Chem.Phys 217, 221 (1997).

[45] A.R. Kolovsky, S.Miyazaki, and R. Graham, Phys.Rev.E 49, 70 (1994).

[46] T. Takami, Phys. Rev. Lett 68, 3371 (1992).

[47] N.W. Ashcroft, N.D. Mermin, in *Solid State Physics*, (Saunders College, Philadelphia, 1976).

[48] R.A. Horn and C.R. Johnson, in *Matrix Analysis*, (Cambridge university press, Cambridge, 1985).

[49] R. Luter, L.E. Reichl, Phys.Rev. A, 66,053615(2002).

[50] M. Gavrila, J.Phys.B: At.Mol.Opt.Phys. 35, R147(2002).

[51] O. Costin, J.L. Lebowitz, A. Rokhlenko, J.Phys.A, 33, 6311(2000).

[52] J.H. Shirley, Phys.Rev., 138, B979(1965).

[53] F.H.M. Faisal, Computer Physics Reports, 9, 55(1989).

[54] J.M. Lopez-Castillo, C. Tannous, J.P. Jay-Gerin, Phys.Rev. A, 41, 2273 (1990).

[55] T. Brandes, J. Robinson, Phys.Stat.Sol (b), 234, 378(2002).

[56] C. Durst, E. Sigmund, P. Reineker, A. Scheuing, J.Phys.C:Solid State, 19, 2701(1986).

[57] D.F. Martinez, L.E. Reichl, G.A. Luna-Acosta, Phys.Rev.B, 66, 174306 (2002).

[58] M. Moskalets, M. Büttiker, Phys.Rev.B, 66, 245321(2002)

[59] H.M. Pastawski, E. Medina, Revista Mexicana de Fisica, 2nd Workshop of Electronic Transport in Mesoscopic Systems, Vol.47, 1(2001); arXiv:cond-mat/0103219, 2001.

[60] K. Haule, J. Bonča, Phys.Rev.B, 59, 13087(1999).

[61] B.K. Ridley, *Quantum Processes in Semiconductors* (Oxford, New York, 1982), Chap. 3.

[62] K. Drese, M. Holthaus, Eur.Phys.J. D, 5, 119(1999)

[63] E.N. Economou, *Green's Functions in Quantum Physics*, (Springer-Verlag, New York, 1979).

Vita

Dario Fernando Martinez Mantilla was born in Bucaramanga, Colombia on 24 February 1971, the son of Ing. Edgard Martinez and Nubia Mantilla. He graduated from Colegio Agustiniano Norte in 1988, participated in the Colombian Physics Olympiad in 1987(third place) and 1988 (second place) and in 1989 participated in the International Physics Olympiad in Poland. In 1989 entered the undergraduate program in Physics at the Universidad de los Andes; in 1993 participated in the Opcion Colombia program working in Cali, Colombia, for the Income Generation Program of the Presidential Program for the Youth (P.P.P.J). In 1994 became part of the Grupo Opcion Colombia-Los Andes and was elected in the advisory board of Opcion Colombia. In 1995 became an executive member of the same corporation. He received a Bachelor of Science degree in Physics from the Universidad de los Andes in Bogota in 1996. He entered the graduate program at the University of Texas at Austin in the same year.

Permanent address: 2614 Deerfoot trail, Austin, TX, 78704

This dissertation was typeset with LaTeX[†] by the author.

[†]LaTeX is a document preparation system developed by Leslie Lamport as a special version of Donald Knuth's TeX Program.